3.5. Tumorigenic activity in viable cells following treatment with LBaP

The tumorigenicity of the cells that survived apoptosis after the treatment with LBaP was evaluated based on (1) the ability to form colonies, (2) the ability to proliferate in low-serum conditions, and 3) the ability to be implanted in mice. Apoptosis induction by serum depletion and cell detachment and treatment with LBaP was repeated three times. The colony-forming ability of normal NIH3T3 cells in soft agar was very poor, but significantly increased in the cells that survived apoptosis by treatment with LBaP (Fig. 6A). As the ability of NIH3T3 to form spontaneous colonies in agar has been reported to increase under the culture conditions as low serum-medium and confluence [24], some parts of colonies formed after LBaP-treatment might be due to spontaneous ones; however, this increase of colony formation would reflect the transformation caused by LBaP-induced inhibition of apoptosis because the appearance rates of colonies and the size were LBaP-dose dependent. In addition, the cells survived by treatment with LBaP showed greater proliferation in low serum conditions, indicating an attenuation of serum-dependency (Supplementary Fig. 4). When normal NIH3T3 cells and viable cells following treatment with LBaP were cultured under low-serum (0.1% and 0.5%) conditions, the latter showed greater proliferation. Furthermore, surviving apoptosis after treatment with LBaP accelerated growth *in vivo* (Fig. 6B). Normal NIH3T3 cells and surviving cells following treatment with LBaP were inoculated subcutaneously into the left leg of nude mice. NIH3T3 cells are established mouse fibroblasts that normally do not form tumors in nude mice. An accelerated tumor growth was observed in mice inoculated with the cells survived following treatment with LBaP. These results indicated that avoiding apoptosis by LBaP transformed the cells.

4. Discussion

BaP is a major carcinogenic PAH. The carcinogenicity of BaP is associated with metabolic activation to reactive diol epoxide intermediates like BPDE and their subsequent covalent binding to critical targets in DNA [1]. Although BaP is known to become toxic when exposed to sunlight [5,6], the carcinogenicity of photooxidized BaP has not been investigated. In this study, we have found that LBaP inhibited apoptosis, and had the potential to generate tumors. This antiapoptotic effect was specific to LBaP, and not observed for BaP itself.

Apoptosis is a physiological cell suicide program critical to the development and maintenance of healthy tissues [25,26]. This evolutionary conserved form of programmed cell death eradicates potentially harmful cells, particularly genetically altered cells. Therefore, dysregulation of apoptosis contributes to tumor progression and malignancy via an accumulation of gene mutations and genetic instability [25,27]. In cancer cells, both the expression of antiapoptotic molecules and the signaling of pro-survival pathways are aberrantly augmented, which promotes their characteristic uncontrolled proliferation and drug resistance. Antiapoptotic effectors such as bcl-2, bcl-xL and survivin were reported to be up-regulated in cancer cells [26,28]. Survival pathways, including the PI3-kinase/Akt, NF-κB, and Ras-Raf-MEK-ERK pathways, were promoted [29,30]. In this study, the antiapoptotic effect was attributable to the production of ROS from LBaP. ROS were reported to activate pro-survival signaling pathways; for example, H_2O_2 induced EGFR tyrosine phosphorylation, resulting in the activation of ERK and Akt pathways [13–16]. We have previously shown that activation of PI3-kinase/Akt by H_2O_2 suppressed the apoptosis caused by serum depletion and cell detachment [19–21]. Although the species of ROS related to the antiapoptosis induced by LBaP are not yet known, the activation of pro-survival signals by ROS generated from LBaP would suppress apoptosis. The fate of cells is decided by a balance between signals for survival and death. Very severe oxidative stress, which sends strong cell death signals, causes cell death and temporary growth arrest, whereas low doses of ROS activate numerous major survival signaling pathways, thereby promoting cell proliferation [31]. This would explain why cells survived at certain doses of LBaP and died at high concentrations.

BaP quinones such as BaP-1,6-dione and BaP-3,6-dione, formed after exposure of BaP to sunlight [2], were reported to activate EGFR through the generation of H_2O_2, leading to cell proliferation in cancer cell line [11]. The activation of the EGFR and PI3-kinase/Akt pathways by BPDE also inhibited apoptosis and acted to promote carcinogenesis [18]. In the present study, many compounds were produced by the degradation of BaP and those with high polarity generated ROS and related antiapoptotic effects; however, BaP-1,6-dione and BaP-3,6-dione were not distributed to the fractions showing antiapoptotic activity. We suspected the contribution of two compounds, BaP-4,5-dihydrodiol and 2-hydroxy-BaP-1,6-dione, considered to produce ROS via redox-cycling [7,10]. BaP-7,8-dione was reported to be 80 times more mutagenic in *p53* than the typical mutagen BPDE, which was attenuated by ROS scavengers [9,10,32]. Multiple effects by many products of oxidized and degraded BaP, which have not yet been identified but could produce ROS, could contribute to the antiapoptotic effects of LBaP and augmented carcinogenicity. PAHs other than BaP were reported to be modified under natural sunlight [33] and SSL [34–36], the altered compounds sometimes showing greater toxicity than the original compounds. Phenanthrene, anthracene and naphthalene were changed to PAH quinones including 9,10-phenanthrenequinone, anthraquinone, hydroquinone, etc. We have previously showed that hydroquinone and benzoquinone showed an antiapoptotic effect similar to LBaP, which was a reason for the tumorigenicity [20]. These results suggested that other PAHs exposed to sunlight have the potential to be carcinogenic by inhibiting apoptosis.

In addition to the inhibition of apoptosis as a reason for the survival of abnormal cells, LBaP itself had the ability to cause genetic damage. We have previously shown that LBaP induced phosphorylation of histone H2AX, which was recently identified as an early event after the induction of DNA double strand breaks (DSBs) [22]. Phosphorylation of histone H2AX induced by LBaP was considered to be due to the DSBs generated by ROS from LBaP and by collision of advancing replication fork with nick or DNA adduct formed by LBaP. Over-expression of an antiapoptotic factor, Bcl-2, promoted genomic instability by inhibiting apoptosis induced by H_2O_2 [37]. The LBaP-induced antiapoptosis shown in this study would enhance the potential for cells genetically altered by the misrepair of DSBs induced by LBaP to survive. Although BaP and some metabolic forms might cause DNA damage, the lack or insufficiency of pro-survival signals triggered by ROS production could decrease the risk of carcinogenicity compared with LBaP.

In conclusion, this study suggests that two important factors need to be considered when examining the risk of environmental chemicals. One is the possibility that exposure to sunlight, may change chemicals to other forms having the potential for more toxicity and carcinogenicity. The other is the antiapoptotic effect, which can lead to an enhancement of carcinogenicity. As typical mutagens and carcinogens like PAHs have not been checked in those points, we encourage adding these two factors to future evaluations of the chemical risks.

Conflict of interest statement

The authors declare that there are no conflicts of interest.

Acknowledgements

This work was supported in part by the Long-range Research Initiative of Japan Chemical Industry Association, the Sumitomo Foundation and a Grant-in-Aid for Scientific Research (C) from the Ministry of Education, Culture, Sports, Science and Technology, Japan [grant number 19510071].

Appendix A. Supplementary data

Supplementary data associated with this article can be found, in the online version, at doi:10.1016/j.cbi.2010.02.044.

References

[1] C.E. Boström, P. Gerde, A. Hanberg, B. Jernström, C. Johansson, T. Kyrklund, A. Rannug, M. Törnqvist, K. Victorin, R. Westerholm, Cancer risk assessment, indicators, and guidelines for polycyclic aromatic hydrocarbons in the ambient air, Environ. Health Perspect. 110 (2002) 451–488.
[2] R. Koeber, J.M. Bayona, R. Niessner, Determination of Benzo[a]pyrene diones in air particulate matter with liquid chromatography mass spectrometry, Environ. Sci. Technol. 33 (1999) 1552–1558.
[3] M. Reed, M. Monske, F. Lauer, S. Meserole, J. Born, S. Burchiel, Benzo[a]pyrene diones are produced by photochemical and enzymatic oxidation and induce concentration-dependent decreases in the proliferative state of human pulmonary epithelial cells, J. Toxicol. Environ. Health A 66 (2003) 1189–1205.
[4] A. Kot-Wasik, D. Dabrowska, J. Namiesnik, Photodegradation and biodegradation study of benzo(a)pyrene in different liquid media, J. Photochem. Photobiol. A: Chem. 168 (2004) 109–115.
[5] X.D. Huang, D.G. Dixon, B.M. Greenberg, Increased Polycyclic Aromatic hydrocarbon toxicity following their photomodification in natural sunlight: impacts on the duckweed Lemna gibba L. G-3, Ecotoxicol. Environ. Safety 32 (1995) 194–200.
[6] M.A. Lampi, J. Gurska, K.I.C. McDonald, F. Xie, X.-D. Huang, D.G. Dixon, B.M. Greenberg, Photoinduced toxicity of polycyclic aromatic hydrocarbons to Daphnia magna: ultraviolet-mediated effects and the toxicity of polycyclic aromatic hydrocarbon photoproducts, Environ. Toxicol. Chem. 25 (2006) 1079–1087.
[7] M.E. Goetz, A. Luch, Reactive species: a cell damaging rout assisting to chemical carcinogens, Cancer Lett. 266 (2008) 73–83.
[8] X. Hu, Y. Zhang, X. Zhao, H.M. Hwang, Biodegradation of benzo[a]pyrene with immobilized laccase: genotoxicity of the products in HaCaT and A3 cells, Environ. Mol. Mutagen. 48 (2007) 106–113.
[9] Y.M. Shen, A.B. Troxel, S. Vedantam, T.M. Penning, J. Field, Comparison of p53 mutations induced by PAH o-quinones with those caused by anti-benzo[a]pyrene diol epoxide in vitro: role of reactive oxygen and biological selection, Chem. Res. Toxicol. 19 (2006) 1441–1450.
[10] D. Yu, J.A. Berlin, T.M. Penning, J. Field, Reactive oxygen species generated by PAH o-quinones cuse change-in-function mutations in p53, Chem. Res. Toxicol. 15 (2002) 832–842.
[11] A.D. Burdick, J.W. Davis, K.J. Liu, L.G. Hudson, H. Shi, M.L. Monske, S.W. Burchiel, Benzo(a)pyrene quinones increase cell proliferation, generate reactive oxygen species, and transactivate the epidermal growth factor receptor in breast epithelial cells, Cancer Res. 63 (2003) 7825–7833.
[12] W.S. Wu, The signaling mechanism of ROS in tumor progression, Cancer Metastasis Rev. 25 (2006) 695–705.
[13] T. Goldkorn, N. Balaban, K. Matsukuma, V. Chea, R. Gould, J. Last, C. Chan, C. Chavez, EGF-receptor phosphorylation and signaling are targeted by H_2O_2 redox stress, Am. J. Respir. Cell. Mol. Biol. 19 (1998) 786–798.
[14] X. Wang, K.D. McCullough, T.F. Franke, N.J. Holbrook, Epidermal growth factor receptor-dependent Akt activation by oxidative stress enhances cell survival, J. Biol. Chem. 275 (2000) 14624–14631.
[15] K.Z. Guyton, Y. Liu, M. Gorospe, Q. Xu, N.J. Holbrook, Activation of mitogen-activated protein kinase by H_2O_2. Role in cell survival following oxidant injury, J. Biol. Chem. 271 (1996) 4138–4142.
[16] G.R. Hayes, D.H. Lockwood, Role of insulin receptor phosphorylation in the insulinomimetic effects of hydrogen peroxide, Proc. Natl. Acad. Sci. U.S.A. 84 (1987) 8115–8119.
[17] L. Rodríguez-Fragoso, K. Melendez, L. Hudson, F. Lauer, S. Burchiel, EGF-receptor phosphorylation and downstream signaling are activated by benzo[a]pyrene 3,6-quinone and benzo[a]pyrene 1,6-quinone in human mammary epithelial cells, Toxicol. Appl. Pharmacol. 235 (2009) 321–328.
[18] A.D. Burdick, I.D. Ivnitski-Steele, F.T. Lauer, S.W. Burchiel, PYK2 mediates anti-apoptotic AKT signaling in response to benzo[a]pyrene diol epoxide in mammary epithelial cells, Carcinogenesis 27 (2006) 2331–2340.
[19] Y. Ibuki, R. Goto, Suppression of apoptosis by UVB irradiation: survival signaling via PI3-kinase/Akt pathway, Biochem. Biophys. Res. Commun. 279 (2000) 872–878.
[20] Y. Ibuki, R. Goto, Dysregulation of apoptosis by benzene metabolites and their relationships with carcinogenesis, Biochim. Biophys. Acta 1690 (2004) 11–21.
[21] Y. Ibuki, M. Akaike, T. Toyooka, R. Goto, Akt1-mediated intracellular oxidation after UVB irradiation suppresses apoptotic cell death induced by cell detachment and serum starvation, Photochem. Photobiol. 84 (2008) 154–161.
[22] T. Toyooka, G. Ohnuki, Y. Ibuki, Solar-simulated light-exposed benzo[a]pyrene induces phosphorylation of histone H2AX, Mutat. Res. 650 (2008) 132–139.
[23] H. Jiang, S.L. Gelhaus, D. Mangal, R.G. Harvey, I.A. Blair, T.M. Penning, Metabolism of benzo[a]pyrene in human bronchoalveolar H358 cells using liquid chromatography–mass spectrometry, Chem. Res. Toxicol. 20 (2007) 1331–1341.
[24] H. Rubin, Selected cell and selective microenvironment in neoplastic development, Cancer Res. 61 (2001) 799–807.
[25] J. Plati, O. Bucur, R. Khosravi-Far, Dysregulation of apoptotic signaling in cancer: molecular mechanisms and therapeutic opportunities, J. Cell. Biochem. 104 (2008) 1124–1149.
[26] J.C. Reed, Dysregulation of apoptosis in cancer, J. Clin. Oncol. 17 (1999) 2941–2953.
[27] D. Hanahan, R.A. Weinberg, The hallmarks of cancer, Cell 100 (2000) 57–70.
[28] S. Kitada, I.M. Pedersen, A.D. Schimmer, J.C. Reed, Dysregulation of apoptosis genes in hematopoietic malignancies, Oncogene 21 (2002) 3459–3474.
[29] K. Breuhahn, T. Longerich, P. Schirmacher, Dysregulation of growth factor signaling in human hepatocellular carcinoma, Oncogene 25 (2006) 3787–3800.
[30] L.Z. Liu, X.W. Hu, C. Xia, J. He, Q. Zhou, X. Shi, J. Fang, B.H. Jiang, Reactive oxygen species regulate epidermal growth factor-induced vascular endothelial growth factor and hypoxia-inducible factor-1alpha expression through activation of AKT and P70S6K1 in human ovarian cancer cells, Free Radic. Biol. Med. 41 (2006) 1521–1533.
[31] J.L. Martindale, N.J. Holbrook, Cellular response to oxidative stress: signaling for suicide and survival, J. Cell. Physiol. 192 (2002) 1–15.
[32] D. Yu, T.M. Penning, J.M. Field, J.A. Berlin, Benzo[a]pyrene-7,8-dione is more mutagenic than anti-BPDE on p53 and is dependent on the generation of reactive oxygen species, Polycyclic Aromatic Compd. 22 (2002) 881–891.
[33] B.J. McConkey, L.M. Hewitt, D.G. Dixon, B.M. Greenberg, Natural sunlight induced photooxidation of naphthalene in aqueous solution, Water Air Soil Pollut. 136 (2002) 347–359.
[34] J. Holt, S. Hothem, H. Howerton, R. Larson, R. Sanford, 9,10-Phenanthrenequinone photoautocatalyzes its formation from phenanthrene, and inhibits biodegradation of naphthalene, J. Environ. Qual. 34 (2005) 462–468.
[35] A. Mallakin, D. George Dixon, B.M. Greenberg, Pathway of anthracene modification under simulated solar radiation, Chemosphere 40 (2000) 1435–1441.
[36] B.J. McConkey, C.L. Duxbury, D.G. Dixon, B.M. Greenberg, Toxicity of a PAH photooxidation product to the bacteria Photobacterium phosphoreum and the duckweed Lemna gibba: effects of phenanthrene and its primary photoproduct, phenanthrenequinone, Environ. Toxicol. Chem. 16 (1997) 892–899.
[37] A.G. Cox, M.B. Hampton, Bcl-2 over-expression promotes genomic instability by inhibiting apoptosis of cells exposed to hydrogen peroxide, Carcinogenesis 28 (2007) 2166–2171.

EDITORIAL COMMENT

This immunohistochemical study revealed that maspin expression was detected in 41.1% of the renal cell carcinoma samples obtained from patients with radical or partial nephrectomy, and its localization was cytoplasmic in all of the positive cases, and cytoplasmic expression of maspin correlates with tumor size in renal cell carcinoma. The authors suggested the possibility of maspin as a biomarker in more invasive renal cell carcinoma.

Maspin was originally identified as a tumor suppressor that affects cell motility and invasion.[1,2] Especially, a series of cellular and molecular studies have shown that maspin is expressed in normal human mammary and prostate epithelial cells but down-regulated during cancer progression.[2] The loss of *maspin* gene expression with increasing malignancy is regulated by the epigenetic mechanism.[3,4] However, some studies have shown that its expression correlated with malignant behavior in some malignancies such as pancreatic, ovarian, and lung cancers, suggesting that maspin might play different roles depending on cell type.[2] In addition, the localization of maspin is thought to be important to its functions. Cytoplasmic expression of maspin coincided with a poor prognosis in ovarian cancers, whereas nuclear expression was detected in benign and low-malignant-potential tumors.[5] As for renal cell carcinoma, there is an only one report (Blandamura et al.) in addition to this study.[6] In previous reports, maspin expression was not detected in kidney cells.[3,4] Thus, tissue distribution and subcellular localization of maspin is the important information. Comparing these two studies, cytoplasmic expression of maspin was detected in 41.1% of samples in this study, whereas it was not detected in Blanamura's study. To clarify this discrepancy, further studies are needed.

Many different clinicopathological factors have been previously investigated for prognosis of renal cell carcinoma.[7] Among these factors, the most consistent and widely investigated factors are stage and histological grade. In this study, the tumor stage was an independent prognostic factor, but maspin expression was not an independent prognostic factor. Surprisingly, cytoplasmic expression of maspin was inversely correlated with tumor size in renal cell carcinoma. This does not coincide with most of the previous studies suggesting the relationship between maspin localization and its functions.[2,8] This result may suggest the complexity of expression, regulation, and function of maspin. Thus further large-scale and reproducible studies are needed to clarify the usefulness of maspin as a prognostic molecular marker.

Masatoshi Watanabe, M.D., Yokohama National University, Hodogaya-ku, Yokohama, Kanagawa Prefecture, Japan

References

1. Zou Z, Anisowicz A, Hendrix MJ, et al. Maspin, a serpin with tumor-suppressing activity in human mammary epithelial cells. *Science*. 1994;263:526-529.
2. Khalkhali-Ellis Z. Maspin: the new frontier. *Clin Cancer Res*. 2006; 12:7279-7283.
3. Futscher BW, Oshiro MM, Wozniak RJ, et al. Role for DNA methylation in the control of cell type specific maspin expression. *Nat Genet*. 2002;31:175-179.
4. Fitzgerald M, Oshiro M, Holtan N, et al. Human pancreatic carcinoma cells activate maspin expression through loss of epigenetic control. *Neoplasia*. 2003;5:427-436.
5. Sood AK, Fletcher MS, Gruman LM, et al. The paradoxical expression of maspin in ovarian carcinoma. *Clin Cancer Res*. 2002;8:2924-2932.
6. Blandamura S, Giacomelli L, Leo G, et al. Nuclear maspin detection in renal cell tumours: possible diagnostic role and correlation with p53 status. *Histopathology*. 2006;49:274-282.
7. Furniss D, Harnden P, Ali N, et al. Prognostic factors for renal cell carcinoma. *Cancer Treat Rev*. 2008;34:407-426.
8. Bailey CM, Khalkhali-Ellis Z, Seftor EA, et al. Biological functions of maspin. *J Cell Physiol*. 2006;209:617-624.

doi:10.1016/j.urology.2010.01.074
UROLOGY 76: e1, 2010. © 2010 Elsevier Inc.

REPLY

Despite numerous studies on maspin expression in malignant tumors, the mechanism of this marker on a molecular basis has not been clearly defined to date. Although maspin was determined to be a marker for good prognosis,[1] it was described as a marker for poor prognosis in some malignant tumors.[2] Although cytoplasmic maspin staining was an indication for poor prognosis in some tumors,[3] in some studies, as was in our study, it was found to be a marker for good prognosis. The literature presents only 1 study on maspin expression in renal tumors.[4] In our study, only cytoplasmic maspin reactivity was determined in renal cell carcinoma samples; however, in the previous study, only nuclear reactivity was observed. Thus, all the specimens used in our study were re-evaluated and it was determined that maspin showed cytoplasmic staining in the normal renal tube epithelium neighboring the tumor.

The differences in the results of our study and an earlier study on maspin expression in renal tumors clearly show the need for further and detailed studies on this subject. One important question that should be addressed is whether different immunohistochemical methods used and different cut-off values reported for maspin expression will lead to such discrepancies in the results. Defining a standard immunohistochemical method and a standard cut-off value in investigations of maspin expression may contribute to resolving this problem. Moreover, future studies on maspin expression in renal cell carcinoma should involve larger series of patients, and, if possible, should be designed to demonstrate the molecular behavior of this marker.

Tahsin Turunc, M.D., and Baris Kuzgunbay, M.D., Department of Urology, Baskent University Faculty of Medicine, Ankara, Turkey

References

1. Zou Z, Anisowicz A, Hendrix MJ, et al. Maspin, a serpin with tumor-supressing activity in human mammary epithelial cells. *Science*. 1994;263:526-529.
2. Bal N, Kocer NE, Ertorer ME, et al. Maspin, E-selectin, and p-selectin expressions in papillary thyroid carcinomas and their correlation with prognostic parameters. *Pathol Res Pract*. 2008;204:743-750.
3. Mohsin SK, Zhang M, Clark GM, et al. Maspin expression in invasive breast cancer: association with other prognostic factors. *J Pathol*. 2003;199:432-435.
4. Blandamura S, Giacomelli L, Leo G, et al. Nuclear maspin dedection in renal cell tumours: possible diagnostic role and correlation with p53 status. *Histopathology*. 2006;49:274-282.

doi:10.1016/j.urology.2010.02.005
UROLOGY 76: e1, 2010. © 2010 Elsevier Inc.

Toxicology in Vitro 24 (2010) 638–644

Contents lists available at ScienceDirect

Toxicology in Vitro

journal homepage: www.elsevier.com/locate/toxinvit

Establishment of yeast reporter assay systems to detect ligands of thyroid hormone receptors α and β

Kazuhiro Shiizaki, Shota Asai, Shingo Ebata, Masanobu Kawanishi, Takashi Yagi *

Environmental Genetics Laboratory, Frontier Science Innovation Center and Graduate School of Science, Osaka Prefecture University, 1-2 Gakuen-cho, Naka-ku, Sakai-City, Osaka 599-8570, Japan

ARTICLE INFO

Article history:
Received 7 November 2008
Accepted 2 October 2009
Available online 22 October 2009

Keywords:
Saccharomyces cerevisiae
Thyroid hormone receptor α, β
Reporter assay
Coactivator
Endocrine disruptors

ABSTRACT

Thyroid hormones are essential for proper development and differentiation in vertebrates. Recently, concern over the disruption of thyroid hormone homeostasis by industrial chemicals and environmental pollutants has been spreading. To evaluate these chemicals, several bioassays have been developed to detect thyroid hormone ligand activity. Nevertheless, a simple and useful assay is required for the assessment of an enormous number of environmental chemicals. We established yeast reporter assays by expression of full-length thyroid hormone receptor (TRα or TRβ) cDNA and of the TR-dependent reporter gene in yeasts. By additional introduction of the general coactivator SRC-1 cDNA into the yeasts, a higher response to endogenous thyroid hormones, thyroxine (T4), and triiodothyronine (T3) was obtained. The EC50 values for T3 were 35 and 1.5 nM for TRα and TRβ assay yeasts, respectively. We tested four chemicals, tetrabromobisphenol A, tetramethylbisphenol A, 2-isopropylphenol, and *o*-*t*-butylphenol, which are suspected to have thyroid hormone-disrupting activity. All four chemicals showed agonistic activities in both assay yeasts; however, their activities were weak in comparison with endogenous TR ligands. Antagonist activities of 2-isopropylphenol and *o*-*t*-butylphenol were also found in the TRα yeast assay. Taken together, these assay yeasts will be powerful tools for assessing TR ligand activity of industrial chemicals and environmental pollutants.

1. Introduction

The thyroid hormones (THs) are widely distributed in a range of vertebrates and are essential for proper development and differentiation. These hormones, thyroxine (T4) and triiodothyronine (T3), are tyrosine-based hormones produced by the thyroid gland. The thyroid hormones regulate energetic homeostasis by increasing the basal metabolic rate affecting protein synthesis and carbohydrate metabolism (Yen, 2001). T4 is the predominant form of THs in the blood and is converted to T3 by deiodinases in the cells. Most biological activities of THs are due to T3 because it has a 10–15-fold higher affinity for binding to thyroid hormone receptors (TRs) than T4 (Togashi et al., 2005). 3,5-Diiodo-L-thyronine (T2) found *in vivo* as a T3 metabolite bound to TR with a very low affinity. Interestingly, T2 can repress TSH gene expression in a similar dose to T3 *in vivo*, so T2 may be involved in the non-TRs pathway (Moreno et al., 2008).

The biological actions of THs are mediated by TRs that are members of a large family of nuclear receptors including steroid hormone receptors (Evans, 1988). The ligand-bound TRs heterodimerize with retinoid X receptor α (RXRα) and can bind to TH response elements (TREs) (Lazar et al., 1990). The TR/RXRα heterodimer causes transcriptional activation of downstream genes of TREs. In addition, transcriptional activation requires recruitment of coactivators such as steroid receptor coactivator-1 (SRC-1) to the TR/RXRα complex (Takeshita et al., 1996). TREs consist of two copies of the consensus motif sequence 5′-AGGTCA-3′ (Brent et al., 1989). A representative TRE that has two copies of the motif arranged as a direct repeat separated by 4 bp is referred to as a DR-4 element (Suen et al., 1994). Another TRE with everted repeats (ER-6) is also common. A third TRE with head-to-head repeats without base pair separation, inverted repeat (IR-0), is less common (Glass et al., 1988). There are two major TR isoforms encoded by different genes, which are designated as TRα and TRβ (Sap et al., 1986; Weinberger et al., 1986; Jansson et al., 1983; Thompson et al., 1987). In mammalian species, TRα and TRβ contain a highly homologous DNA-binding domain (DBD) and a ligand-binding domain (86% and 82%, respectively, in amino acid sequences) (Lazar et al., 1990). Both TR isoforms bind to T3 and mediate TH-regulated gene expression, but their physiological functions are not the same. Mice with null mutant or dominant negative mutant of each receptor display different phenotypes. The inactivation of the TRβ gene leads to hyperthyroxinemia by

* Corresponding author. Tel.: +81 72 254 9862; fax: +81 72 254 9938.
E-mail address: yagi-t@riast.osakafu-u.ac.jp (T. Yagi).

0887-2333/$ - see front matter © 2009 Elsevier Ltd. All rights reserved.
doi:10.1016/j.tiv.2009.10.001

the disorder of the pituitary–thyroid axis, while TRα null mice have normal thyroid hormone and TSH levels. TRα null mice represent lower heart rate and body temperature (Wikstrom et al., 1998). TRβ null mice defect the auditory function (Forrest et al., 1996).

The ligands capable of binding to TRs are not only endogenous T3 and T4. Several classes of environmental chemicals have a high degree of structural similarity to the THs, and interfere with the binding of THs to TRs (Zoeller, 2005). Polychlorinated biphenyls (PCBs) can bind to TRα and TRβ as antagonists, and disturb TR-mediated transcription (Shiraishi et al., 2003). Recently, it was reported that the polybrominated and polychlorinated diphenylethers, 3,3′,5-trichlorobisphenol A, 3,3′,5-tribromobisphenol A, and 3,3′-dibromobisphenol A, commercially available as fire retardants, have antagonistic activity to TRs (Kitamura et al., 2005; Ghisari et al., 2005; Kudo et al., 2005). TH homeostasis is highly regulated by several protein factors including pituitary peptide hormone TSH and hypothalamus peptide hormone TRH. Because TRs play a key role in TH homeostasis by negative and positive regulation of these protein factors through gene transcription (Chatterjee et al., 1989; Darling et al., 1989; Hollenberg et al., 1995), disruption of TH homeostasis by these exogenous TR ligands is of great concern. Moreover, the differences in function of TRα and TRβ indicate that TH-like activities of chemicals should be assessed by both receptor subtypes individually.

Several *in vitro* bioassays have been developed for the screening of TR ligands. These bioassays are based on quantification of a reporter enzyme as a consequence of nuclear receptor activation in mammalian cells or yeasts (Zoeller, 2005; Jugan et al., 2007; Walfish et al., 1997; Li et al., 2008; Moriyama et al., 2002). These assays have the advantages of being fast and relatively simple. Furthermore, yeast-based bioassays are more cost-effective and easier to handle than mammalian cell-based bioassays. However, all of the reported yeast assays are based on the yeast two-hybrid assay system using the only ligand-binding domain of TRs. We attempted to establish yeast reporter assay systems with "intact" human TRs and coactivator resembling to human cell. In this study, we developed novel reporter yeasts for screening TRα and TRβ ligands with intact TRs and SRC-1, and examined their responses to endogenous THs and chemicals which are suspected to be TR ligands.

2. Materials and methods

2.1. Chemicals

Dimethyl sulfoxide (DMSO), dithiothreitol (DTT), and *o*-nitrophenol-β-D-galactopyranoside (ONPG) were purchased from WAKO Pure Chemical (Osaka, Japan). 3,5-Diiodothyronine (T2), 3,5,3′-triiodothyronine (T3), and 3,5,3′,5′-tetraiodothyronine (T4) were obtained from Sigma Aldrich Chemical Co. (St. Louis, MO, USA). Tetrabromobisphenol A (TBBPA), tetramethylbisphenol A (TMBPA), and 2-isopropylphenol (IPP) were purchased from Tokyo-Kasei (Tokyo, Japan). *o-t*-Butylphenol (OBP) was purchased from Nacalai Tesque (Kyoto, Japan). Restriction enzymes, DNA modification enzymes, and other chemicals were obtained from WAKO Pure Chemical (Osaka, Japan).

2.2. Plasmids

The nuclear receptor expression vector, the coactivator expression vector, and the reporter vector were constructed for the development of TRα and TRβ reporter assays. The nuclear receptor expression vector pUdp6 was constructed as follows. The DNA fragment encoding the yeast *ura3* gene was digested using pESC-ura vector (Invitrogen, Carlsbad, CA) and cloned into pUC18 (Takara Bio, Shiga, Japan). Then, the DNA fragment containing the gal1/gal10 dual directional promoter of YEplac181 (Gietz et al., 1988) was cut and inserted into the vector described above. Two DNA fragments containing the yeast *ADH* terminator and the yeast *cyc1* terminator were amplified by PCR from yeast genomic DNA and inserted downstream of the gal1 and gal10 promoter, respectively. A detailed map of the vector is shown in Fig. 1.

Human TRα, TRβ, and RXRα cDNA were amplified from human mammary gland cDNA (Clontech, Palo Alto, CA) with the primer pairs shown in Table 1. Each cDNA was re-amplified with primers containing a restriction site and/or the yeast ribosomal binding consensus sequence near the initiation codon, and cloned into the multi-cloning site (MCS1 or MCS2) of the pUdp6 vector. The plasmid vector pUdp6-TRα/RXRα contains TRα and RXRα cDNAs in MCS1 and MCS2, respectively. The plasmid vectors pUdp6-TRα and pUdp6-TRβ contain only TRα or TRβ cDNA in MCS1, respectively. To construct the human SRC-1e expression vector, SRC-1e cDNA was amplified by PCR from the cDNA described above and cloned into MCS1 in the pESC-leu vector (Invitrogen, Carlsbad, CA). The reporter vector pRW95-3 includes the TRP-1 selection marker, the yeast Cen6 origin for episomal replication, and the LacZ gene located immediately downstream the cyc1 minimum promoter. The double-stranded oligonucleotide containing the TRE (Table 1) was phosphorylated and inserted upstream of the cyc1 minimal promoter in the pRW95-3 vector (Wolf et al., 1996). Each plasmid vector pYT-DR4×3, pYT-ER6×3, and pYT-IR0×3 contained three copies of DR-4, ER-6, and IR-3 oligonucleotides, respectively. To construct the control reporter vector pYT-cyc expressing β-galactosidase constitutively, the DNA fragment corresponding to the 5′-flanking region of the cyc1 gene was amplified with primer pairs (Table 1), and inserted upstream of the cyc1 minimal promoter of the pWE95-3 vector.

2.3. Yeast strain and transformation

Saccharomyces cerevisiae strain W303a (MAT**a**, *ade*2-1, *trp*1-1, *leu*2-3, *his*3-11, 15, *ura*3-1) was used throughout the experiment. Cells were cultured in synthetic complete medium consisting of 0.67% yeast nitrogen base without amino acids (Difco, Detroit, MI), 2% glucose, and appropriate supplements. Drop-out medium was prepared by excluding the indicated nutrient from the synthetic complete medium. All transformations were performed following the lithium acetate method (Ito et al., 1983). First, the reporter vector was introduced into the yeasts and selected on trp- plates. A single colony was isolated and cultured in trp⁻ medium. Second, the nuclear receptor expression plasmid was linearized by *EcoRV* and introduced into the yeasts by homologous recombi-

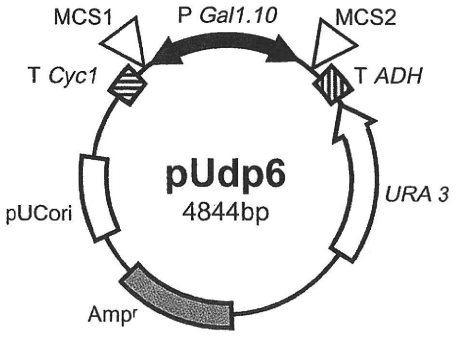

Fig. 1. Plasmid map of pUdp6 vector. Yeast *ura*3 gene (*URA*3), gal1,10 dual directional promoter of YEplac181 (P *Gal*1,10), terminator sequence of yeast alcohol dehydrogenase (T *ADH*) and terminator sequence of yeast cytochrome C (T *Cyc*) were inserted into the parental vector pUC19. TRα or TRβ cDNA were inserted in the multiple cloning site 1 (MCS1) and RXRα cDNA was cloned into the multiple cloning site 2 (MCS2).

Table 1
Oligonucleotides used in the study.

Primers for nuclear receptor and coactivator cDNA amplification	
TRaF	GTGAATGGAACAGAAGCCAAGCAAGG
TRaR	GGCCGCCTGAGGCTTTAGACTTCC
TraRbSpF	GGGCACTAGTAACAAAATGGAACAGAAGCCAAGCA
TraHdR	GGCCAAGCTTGCTTTAGACTTCCTGATCCTCAAAG
TRbF	TAACCTATGACTCCCAACAGTATGACAG
TRbRbSpF	CAGGACTAGTAAACTATGACTCCCAACAGTATGAC
TRbR	TCAGTCTAATCCTCGAACACTTCCAAG
TRbHdR	TTCGTGAAGCTTCAGTCTAATCCTCGAACACTTCC
RXRaEcr	CTTAAGAATTCTAAGTCATTTGGTGCGGC
RXRaKpf	CATTAGGTACCATGGACACCAAACATTTCC
SRC-1eFbg2	CAAAGAAGATCTCCCAGGTGTGAAG
SRC-1eRxh2	AGGGCCCTCGAGACTCTAGTCTGTAG
Oligo nucleotides for TR response element in reporter gene	
DR4-Nh	CTAGCAGGTCACAGGAGGTCAGATGCT
DR4-XB	CTAGAGCATCTGACCTCCTGTGACCTG
IR0Xba	CTAGATCTCAGGTCATGACCTTTCATCCA
IR0Spe	CTAGTGGATGAAAGGTCATGACCTGAGAT
ER-6Xb	CTAGAATATGACCTCAAAGGAGGTCAGTGG
ER-6Nh	CTAGCCACTGACCTCCTTTGAGGTCATATT
Primers for cyc1 promoter amplification	
CYCpf	ATTTGGCGAGCGTTGGTTGG
CYCpr	GCATGCCATATGATCATGTGTC

Consensus half-sites for TRs binding are underlined.

nation. Transformed cells were selected and maintained in the *ura*$^-$ and *trp*$^-$ medium as a heterogeneous population. Finally, the SRC-1 expression plasmid was introduced into the yeasts and selected for using the ura$^-$, trp$^-$, leu$^-$ plates. The control vector pYT-cyc was introduced into yeasts and selected for using the trp$^-$ plates.

2.4. Reporter assay

The assay procedure was similar to that described by Miller (1998). The yeast strains were grown overnight at 30 °C in a synthetic glucose medium lacking tryptophan, uracil, and leucine. A 1 μl aliquot of the test chemical dissolved in dimethylsulfoxide (DMSO), 5 μl of the overnight culture yeasts, and 100 μl of synthetic medium containing 2% galactose were mixed in each well of a 96-well microtiter plate with subsequent incubation for 16 h at 30 °C. For determination of agonist effect, various concentration of THs and chemicals were used; 10^{-9}–10^{-4} M T2, T3, and T4; 10^{-8}–10^{-4} M OBP; 10^{-7}–10^{-3} M IPP; 10^{-9}–10^{-4} M TBBPA; and 10^{-9}–10^{-4} M TMBPA. In order to confirm the antagonist effects of the above chemicals, 35 and 1.5 nM T3 were mixed to them in TRα and TRβ yeast assays, respectively.

Each cell suspension (10 μl) was transferred to a new 96-well microtiter plate and 100 μl of Z-buffer (60 mM Na_2HPO_4, 40 mM NaH_2PO_4, 1 mM $MgCl_2$, 10 mM KCl, 2 mM dithiothreitol, and 0.2% sarcosyl, adjusted to pH 7) containing 1 mg/ml *o*-nitrophenol-β-D-galactopyranoside (ONPG) was added to the plate with subsequent incubation for 60 min at 37 °C. The absorbance at 405 and 595 nm was measured, to indicate the amount of *o*-nitrophenol generated and the yeast cell density, respectively. The relative β-galactosidase activity was represented by a ratio of 405–595 nm absorbance.

2.5. Statistical analysis

The data were analyzed by ANOVA with a Duncan's post-hoc test to assess significance of the values. Probability (p) values < 0.05 were considered statistically significant.

3. Results

3.1. Optimization of TRE and reporter gene arrangement

We tested reporter gene constructs containing three different TH response elements (TREs), DR-4, ER-6, and IR-0. We introduced the plasmid expressing both TRα and RXRα into the yeasts containing the reporter plasmid with DR-4-type TREs. As it is reported that TRs can bind as homodimers to ER-6 and IR-0-type TREs, we also introduced the plasmid expressing TRα but not RXRα into the yeasts with the reporter plasmid containing ER-6 and IR-0-type TREs. Among them, expression of the reporter gene only containing IR-0 was induced at a low level by 10 μM T3 in TRα-expressing yeasts (Fig. 2). We also tested the expression of other reporter genes with various copy numbers of DR-4 and ER-6-type TREs, but none of these reporter genes responded to T3 (data not shown). Similarly, expression of the reporter gene with IR-0-type TRE represented higher induction by T3 in the TRβ-expressing yeasts (Fig. 2). We concluded that reporter enzyme activity depends on the copy number of the IR-0-type TRE in the reporter vector. The reporter plasmid pYT-IR-0×5 containing five copies of IR-0-type TRE showed the highest reporter activity. We therefore used pYT-IR-0×5 as a reporter plasmid to establish TRα and TRβ reporter assay yeasts.

3.2. Effects of coactivator expression

We introduced the SRC-1-expressing plasmid into the reporter yeasts to examine whether the coactivator could enhance reporter gene expression. As shown in Fig. 3, the expression of SRC-1 significantly enhanced the response to T3 in the reporter yeasts. The yeasts expressing SRC-1 showed a lower detection limit of T3 concentration than that of the yeasts without SRC-1 expression. The detection limits of T3 were 2 and 0.2 nmol/L in the TRα and TRβ assay yeasts, respectively. The maximum induction level of β-galactosidase was also enhanced by the expression of SRC-1 in the yeast. The β-galactosidase activity increased 10- and 6-fold in the TRα and TRβ assay yeasts, respectively, through the addition of 1 μmol/L T3. We selected typical clones representing higher β-galactosidase activity induced by T3 exposure, and further investigated their responses to endogenous and exogenous TR ligands.

3.3. Response to thyroid hormones

Fig. 4 represents the dose–response curves of reporter expression against THs in the TRα and TRβ assay yeasts. The EC50 values of THs calculated from the dose–response curves are shown in Ta-

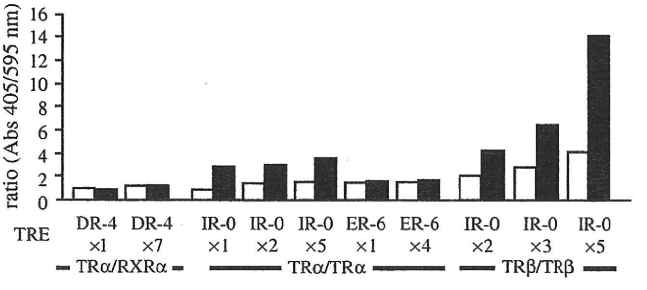

Fig. 2. Response to T3 in yeasts containing various reporter plasmids with different TREs. Reporter plasmids containing DR-4-type TRE were introduced into the yeast coexpressing TRα and RXRα (TRα/RXRα). Reporter plasmids containing IR-0- or ER-6-type TREs were introduced into the yeast expressing only TRα or TRβ (TRα/TRα and TRβ/TRβ). Data are the results from a representative yeast clone from at least 16 individual clones. Open column: solvent control (DMSO). Closed column: 10 μM T3. Each column represents the average from duplicate experiments.

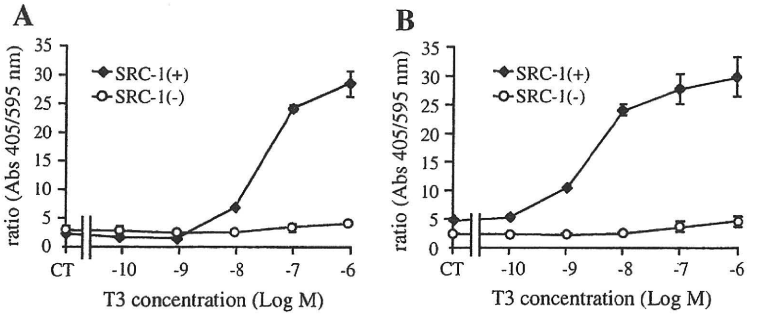

Fig. 3. Enhancement of T3 response by SRC-1 expression in TRα (A) and TRβ (B) reporter assay yeasts. Yeast clones with (■) or without (□) the SRC-1 expression plasmid were exposed to various concentrations (10^{-9}–10^{-4} M) of T3 for 16 h and β-galactosidase activity was measured. Data represent mean ± S.D. of triplicate experiments.

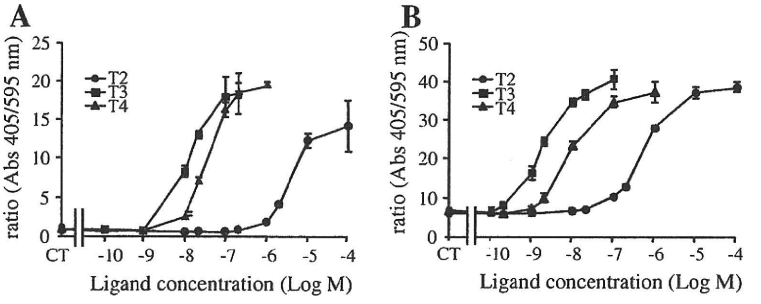

Fig. 4. Responses to THs in TRα (A) and TRβ (B) reporter assay yeasts. The yeasts were exposed to various concentrations (10^{-9}–10^{-4} M) of T2 (●), T3 (■), or T4 (♦) for 16 h and β-galactosidase activity was measured. Data represent mean ± S.D. of triplicate experiments.

Table 2
EC50 of thyroid hormones in TRα and TRβ assay yeasts.

	EC50 (nM)		
Receptor	T2	T3	T4
TRα	7200	35	110
TRβ	870	1.5	9.4

T2:3,5-diiodo-L-thyronine, T3:triiodothyronine, T4:thyroxine.

ble 2. T3 is the most potent ligand, and T4 and T2 are less potent than T3 for both TRα and TRβ assay yeasts. The TRβ assay yeast showed higher sensitivity to all THs than the TRα assay yeast.

3.4. Response to chemicals

We tested several chemicals suspected to be agonists and/or antagonists of TRs by using the established assay yeasts (Figs. 5 and 6). All chemicals tested showed agonist activity with both TRα and TRβ assay yeasts. In contrast to endogenous TRs ligand, these activities were observed only in high doses (>10^{-6} M) of the test chemicals (Figs. 4–6). In three chemicals except TBBPA, the concentrations representing agonistic activity were at least 10-times higher in the TRα yeast assay than that in the TRβ yeast assay (Figs. 5 and 6). On the other hand, TBBPA represented agonistic activity as low as 1 μM in both assay yeasts (Fig. 6A and C). Among the chemicals tested, the most potent ligand was TBBPA, and its maximum agonistic activity was observed at 2 μM in both TRα and TRβ assay yeasts (Fig. 6A and C). These agonist activities were 10-times more potent than the activity of TMBPA that has methyl groups instead of bromides in the bisphenol structure (Fig. 6B and D).

We also investigated antagonist activity of these chemicals by simultaneous exposure to 35 and 1.5 nM T3 for TRα and TRβ assay yeasts, respectively (Figs. 5 and 6). TBBPA and TMBPA showed additive effects in the TRβ assay yeast, while only TMBPA showed additive effects in the TRα assay yeast (Fig. 6). In contrast, OBP higher than 30 μM reduced the reporter gene activity in the TRα assay yeast (Fig. 5A). IPP higher than 100 μM was found to reduce the reporter gene activity in both TRα and TRβ assay yeasts (Fig. 5B and D). At the concentrations up to 50 μM of OBP and to 500 μM of IPP, no transcriptional repression of constitutive β-galactosidase activity was found in the control reporter yeast (Fig. 5E and F), indicating that OBP and IPP had antagonist activity.

Higher concentrations of TBBPA (⩾5 μM) and TMBPA (100 μM) significantly reduced T3-induced reporter gene activity in both TRα and TRβ assay yeasts (Fig. 6A–D). However, this reduction was coincident with the reduction of the constitutive β-galactosidase activity in the control reporter yeast, it may due to cytotoxicity or nonspecific transcriptional repression, but not antagonist activity (Fig. 6E and F).

4. Discussion

To date, several yeast reporter assay systems to detect nuclear receptor ligands have been developed. Most assays adopt the yeast two-hybrid system by using a fusion protein consisting of the ligand-binding domain of the nuclear receptor and the Gal4 DNA-binding domain. We attempted to construct a yeast reporter assay that was as similar as possible to the human cellular process with an intact nuclear receptor. In our laboratory, several yeast reporter assay systems with intact mammalian nuclear receptors have been developed (Kawanishi et al., 2003, 2006, 2008). In the course of these studies, we found that the regulation of the expression level of the cellular components was important for optimization of the assay system. We therefore used three classes of plasmids with different replication origins to construct recombinant assay yeasts in this study. First, the nuclear receptor in the vector without the yeast replication origin was introduced into yeasts by homologous recombination. This vector is integrated into the yeast genome and

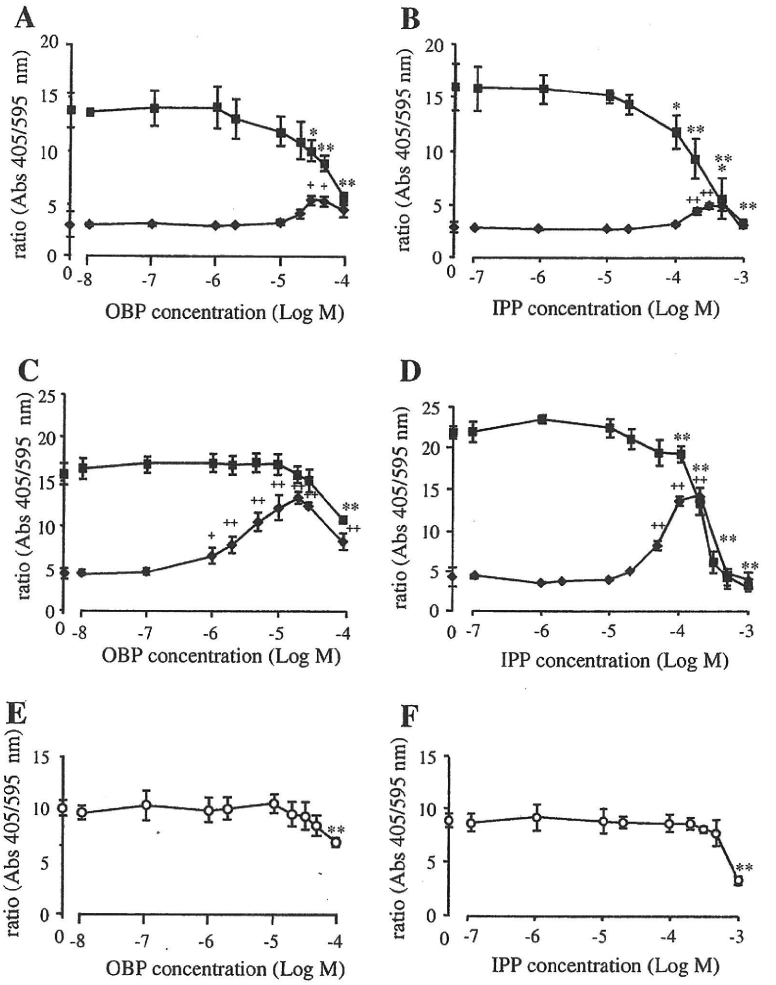

Fig. 5. Responses to phenol compounds in TRα (A and B), TRβ (C and D) and control (E and F) reporter assay yeasts. The yeasts were exposed with 10^{-8}–10^{-4} M *o-t*-butylphenol (OBP: A, C, E) or 10^{-7}–10^{-3} M 2-isopropylphenol (IPP: B, D, F). Agonist activity was measured by exposure to OBP or IPP alone (♦) for 16 h. To determine antagonist effects, 35 and 1.5 nM T3 were added to the above concentration of chemicals in TRα and TRβ yeast assays, respectively (■). In the antagonist assay, results from control assay yeasts expressing β-galactosidase constitutively are also plotted (○). Data represent mean ± S.D. of triplicate experiments. In the agonist assay, statistically significant differences were $^{+}p < 0.05$, $^{++}p < 0.01$ vs. solvent control (by ANOVA, Duncan's post-hoc tests). In the antagonist assay and the control reporter yeast assay, $^{*}p < 0.05$, $^{**}p < 0.01$ vs control (only T3, without test chemicals).

stably expresses the appropriate amount of the nuclear receptor. Second, a reporter plasmid containing β-galactosidase and the yeast cen6 replication origin was constructed. This plasmid is maintained at one or two molecules in each yeast cell and expresses a low amount of the reporter gene product. Third, the episomal plasmid containing the yeast 2-μm replication origin and the coactivator SRC-1e, the major transcript of SRC-1 (Hayashi et al., 1997) was constructed. This plasmid is maintained with high copy numbers in each cell. As a result of these optimizations, we finally succeeded in establishing TRα and TRβ reporter yeasts that are highly responsive to their ligands.

As shown in Fig. 2, no significant induction of the reporter gene activity was observed in both TRα- and TRβ-expressing yeasts carrying DR-4- or ER-6-type TRE, regardless of the multiple copy numbers of responsive elements. Only in yeasts containing IR-0-type TRE was the reporter gene activity induced by T3, although this responsive element is uncommon. It has been reported that the TR/RXRα heterodimer binds to DR-4-type responsive elements, whereas TRα/TRα and TRβ/TRβ homodimers bind to IR-0- and ER-6-type TRE. We tested other combinations of TR expression vectors and TREs, i.e., TRα and DR-4, and TRβ and DR-4, but none of them showed a response to T3. We also constructed a yeast strain with the reporter gene carrying the DR-1 responsive element to confirm RXRα homodimer function. In this yeast, an RXR ligand, 9-*cis* retinoic acid, significantly induced reporter gene activity, suggesting that the inefficient activity of TR/RXRα heterodimers was not due to RXRα (data not shown). We used IR-0-type TRE as an enhancer of the reporter vector, because it is highly responsive to T3 in TR-expressing yeasts and able to avoid the influence of RXRα ligands. As shown in Fig. 3, the additional expression of SRC-1e dramatically enhanced T3-induced reporter gene activity in both TRα- and TRβ-expressing yeasts. Among these yeasts, typical clones were selected for characterization as TRα and TRβ reporter assay strains. The responses to endogenous ligands correlated well to those of mammalian cells (Samuels et al., 1974; Ichikawa et al., 1987), that is, T3 is the most potent ligand followed by T4 and T2 (Fig. 3 and Table 2). T2 is 500 times less potent than T3, and the results were coincident with the previously report (Ball et al., 1997). The TRβ assay yeast showed higher sensitivity to all THs than the TRα assay yeast. Ball et al. (1997) showed that the binding assay of *in vitro* translated TRβ is more responsive to THs than that of TRα. Our data were consistent with the results of these reports.

The reporter assays shown in this study are not so sensitive compared with other bioassays such as *in vivo* assay using the *Xenopus laevis* (Kudo et al., 2005). The reasons may involve reporter gene and its substrates. We used β-galactosidase as a reporter gene

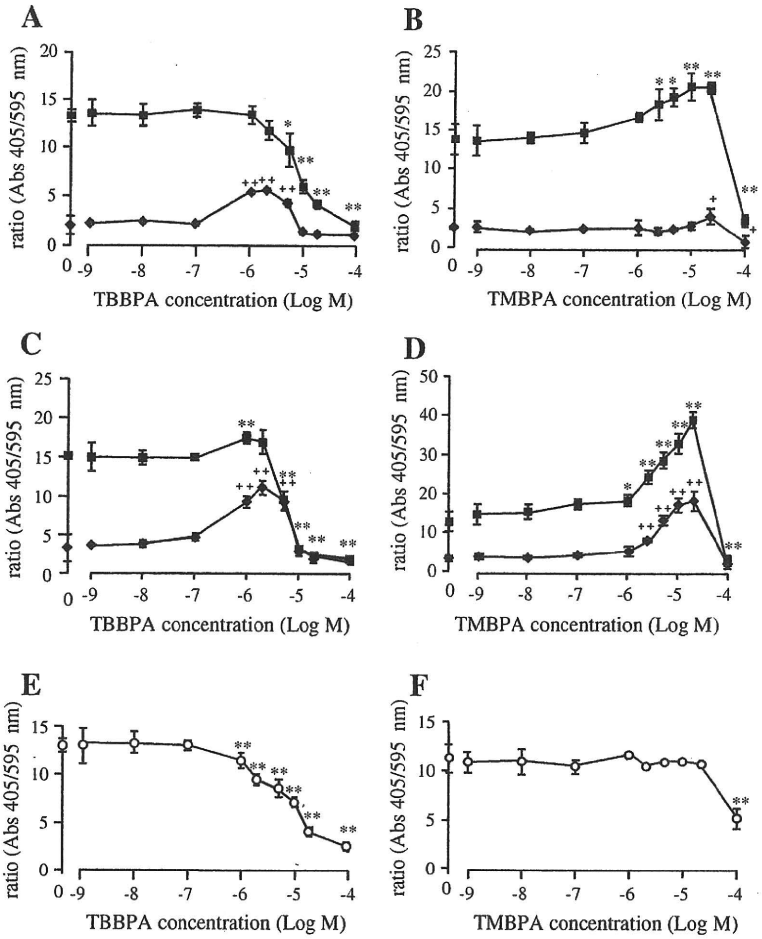

Fig. 6. Responses to phenolic compounds in TRα (A and B), TRβ (C and D), and control (E and F) reporter assay yeasts. The yeasts were exposed to 10^{-9}–10^{-4} M tetrabromobisphenol (TBBPA: A, C, E) or 10^{-9}–10^{-4} M tetramethylbisphenol A (TMBPA: B, D, F). Agonist activity was measured by exposure to TBBPA or TMBPA alone (♦) for 16 h. To determine antagonist effects, 35 and 1.5 nM T3 were added to the above concentration of chemicals in TRα and TRβ yeast assays, respectively (■). In the antagonist assay, results from control assay yeasts expressing β-galactosidase constitutively are also plotted (○). Data represent mean ± S.D. of triplicate experiments. In the agonist assay, statistically significant differences were $^{+}p < 0.05$, $^{++}p < 0.01$ vs. solvent control (by ANOVA, Duncan's post-hoc tests). In the antagonist assay and the control reporter yeast assay, $^{*}p < 0.05$, $^{**}p < 0.01$ vs control (only T3, without test chemicals).

because activity of this enzyme can detect without complex extraction procedure. Other highly sensitive reporter gene such as firefly luciferase may be also available. However, extraction procedure of the luciferase from yeast is complicated and its substrate is expensive. Among β-galactosidase substrates, general order of sensitivity is ONPG < X-Gal < CPRG < luminogenic substrates. We used ONPG as a substrate for detection of β-galactosidase activity because the substrate was most cost-effective, and it did not need expensive equipments for measurement. If higher sensitivity of reporter assays is required, it could be accomplished by using other substrates.

Four industrial chemicals suspected to be TR ligands showed agonistic activity against both TRα and TRβ assay yeasts (Figs. 5 and 6). However, their ligand potencies and specificities to TR subtypes were different. Interestingly, only TBBPA represented similar dose-dependent effects in the TRα and TRβ assay yeasts. The three other chemicals were more potent in the TRβ than the TRα assay yeasts. These results may be due to differences in the ligand-binding domains (AF2 or E/F domain) between TRα and TRβ. As the homology between TRα and TRβ is 86% in the ligand-binding domain, a few critical amino acids could be responsible for the ligand specificity (Wagner et al., 2001; Ye et al., 2003; Baxter et al., 2001).

We also tested whether these assay yeasts can elucidate antagonist activity. Antagonist ligands block the binding of agonist to the nuclear receptor by competition. Agonist ligands promote coactivator binding while antagonists block coactivator binding by inducing a conformational change of the receptor. The antagonist effects can be seen in the existence of coactivator and moderate concentration of agonist ligand. Our assay yeasts were expected to detect antagonist activity because SRC-1, a general coactivator, had been introduced.

In the yeast assay of simultaneous exposure to the chemicals with T3, all four chemicals repressed T3-induced expression in high doses. However, it is difficult to discern whether the repression is due to antagonist activity or nonspecific transcriptional repression of the chemicals tested. To clarify this perplexing result, we developed a reporter assay yeast strain that constitutively expresses β-galactosidase under the control of 5′-flanking region of cyc1 gene. In this control assay yeast, TMBPA and TBBPA repressed constitutive reporter gene activity in a similar manner to the TH-dependent TR assay yeasts, suggesting that these chemicals cause nonspecific transcriptional repression. On the other hand, IPP and OBP represented only weak repression of the constitutive reporter activity even in high doses (Fig. 5). Moreover, antagonistic activity of 100–500 μM of IPP was observed when mixed with T3, while IPP alone showed agonistic activity at the same concentration (Fig. 5B and D). A similar aspect was observed with OBP exposure to the TRα assay yeast but not to the TRβ assay yeast (Fig. 5A and C).

Previous report using the *X. laevis* bioassay showed that these two chemicals had antagonist activities to *Xenopus* TR (Kudo et al., 2005). We concluded that these two chemicals have antagonist activities to human TRs as well as *Xenopus* TR.

In this study, recombinant yeast reporter assay systems to measure TRα and TRβ ligand activities were constructed. The most important element of these assays is the expression of the SRC-1, which accomplishes higher inducibility of ligand-dependent transcription of the reporter gene. This reporter assay has many advantages compared to other assays. It is easy to handle and able to rapidly detect agonists as well as antagonists. This assay will be a powerful tool for assessment of TR ligand activity of industrial chemicals and environmental pollutants.

Acknowledgments

We are grateful to Mrs. Wai-Ling Chu for editing the English in the manuscript. This work was supported in part by an Industrial Technology Research Grant Program in 2005 from the New Energy and Industrial Technology Development Organization (NEDO), and by Science and Technology Incubation Program in Advanced Regions in 2009 from Japan Science and Technology Agency (JST).

References

Ball, S.G., Sokolov, J., Chin, W.W., 1997. 3,5-Diiodo-L-thyronine (T2) has selective thyromimetic effects in vivo and in vitro. J. Mol. Endocrinol. 19, 137–147.

Baxter, J.D., Dillmann, W.H., West, B.L., Huber, R., Furlow, J.D., Fletterick, R.J., Webb, P., Apriletti, J.W., Scanlan, T.S., 2001. Selective modulation of thyroid hormone receptor action. J. Steroid Biochem. Mol. Biol. 76, 31–42.

Brent, G.A., Harney, J.W., Chen, Y., Warne, R.L., Moore, D.D., Reed-Larsen, P., 1989. Mutations of the rat growth hormone promoter which increase and decrease response to thyroid hormone define a consensus thyroid hormone response element. Mol. Endocrinol. 3, 1996–2004.

Chatterjee, V.K., Lee, J.K., Rentoumis, A., Jameson, J.L., 1989. Negative regulation of the thyroid-stimulating hormone alpha gene by thyroid hormone: receptor interaction adjacent to the TATA box. Proc. Natl. Acad. Sci. USA 86, 9114–9118.

Darling, D.S., Burnside, J., Chin, W.W., 1989. Binding of thyroid hormone receptors to the rat thyrotropin-beta gene. Mol. Endocrinol. 3, 1359–1368.

Evans, R.M., 1988. The steroid and thyroid hormone receptor superfamily. Science 240, 889–895.

Forrest, D., Hanebuth, E., Smeyne, R.J., Everds, N., Stewart, C.L., Wehner, J.M., Curran, T., 1996. Recessive resistance to thyroid hormone in mice lacking thyroid hormone receptor β: evidence for tissue-specific modulation of receptor function. EMBO J. 15, 3006–3015.

Ghisari, M., Bonefeld-Jorgensen, E.C., 2005. Impact of environmental chemicals on the thyroid hormone function in pituitary rat GH3 cells. Mol. Cell. Endocrinol. 244, 31–41.

Gietz, R.D., Sugino, A., 1988. New yeast–*Escherichia coli* shuttle vectors constructed with in vitro mutagenized yeast genes lacking six-base pair restriction sites. Gene 74, 527–534.

Glass, C.K., Holloway, J.M., Devary, O.V., Rosenfeld, M.G., 1988. The thyroid hormone receptor binds with opposite transcriptional effects to a common sequence motif in thyroid hormone and estrogen response elements. Cell 54, 313–323.

Hayashi, Y., Ohmori, S., Ito, T., Seo, H., 1997. A splicing variant of steroid receptor coactivator-1 (SRC-1E): the major isoform of SRC-1 to mediate thyroid hormone action. Biochem. Biophys. Res. Commun. 236, 83–87.

Hollenberg, A.N., Monden, T., Flynn, T.R., Boers, M.E., Cohen, O., Wondisford, F.E., 1995. The human thyrotropin-releasing hormone gene is regulated by thyroid hormone through two distinct classes of negative thyroid hormone response elements. Mol. Endocrinol. 9, 540–550.

Ichikawa, K., DeGroot, L.J., 1987. Purification and characterization of rat liver nuclear thyroid hormone receptors. Proc. Natl. Acad. Sci. USA 84, 3420–3424.

Ito, H., Fukada, Y., Murata, K., Kimura, A., 1983. Transformation of intact yeast cells treated with alkali cations. J. Bacteriol. 153, 163–168.

Jansson, M., Philipson, L., Vennstrom, B., 1983. Isolation and characterization of multiple human genes homologous to the oncogenes of avian erythroblastosis virus. EMBO J. 2, 561–565.

Jugan, M.L., Levy-Bimbot, M., Pomerance, M., Tamisier-Karolak, S., Blondeau, J.P., Levi, Y., 2007. A new bioluminescent cellular assay to measure the transcriptional effects of chemicals that modulate the alpha-1 thyroid hormone receptor. Toxicol. In Vitro 21, 1197–1205.

Kawanishi, M., Sakamoto, M., Ito, A., Kishi, K., Yagi, T., 2003. Construction of reporter yeasts for mouse aryl hydrocarbon receptor ligand activity. Mutat. Res. 540, 99–105.

Kawanishi, M., Sakamoto, M., Ito, A., Shimohara, C., Yagi, T., 2006. Establishment of reporter yeasts for guinea pig and syrian hamster aryl hydrocarbon receptor ligand activity. Genes Environ. 28, 167–172.

Kawanishi, M., Kondo, M., Shiizaki, K., Chu, W.L., Terasoma, Y., Yagi, T., 2008. Construction of a reporter yeast strain to detect estrogen receptor signaling through aryl hydrocarbon receptor activation. Environ. Sci. Technol. 42, 6897–6902.

Kitamura, S., Kato, T., Iida, M., Jinno, N., Suzuki, T., Ohta, S., Fujimoto, N., Hanada, H., Kashiwagi, K., Kashiwagi, A., 2005. Anti-thyroid hormonal activity of tetrabromobisphenol A, a flame retardant, and related compounds: Affinity to the mammalian thyroid hormone receptor, and effect on tadpole metamorphosis. Life Sci. 76, 1589–1601.

Kudo, Y., Yamauchi, K., 2005. In vitro and in vivo analysis of the thyroid disrupting activities of phenolic and phenol compounds in *Xenopus laevis*. Toxicol. Sci. 84, 29–37.

Lazar, M.A., Chin, W.W., 1990. Nuclear thyroid hormone receptors. J. Clin. Invest. 86, 1777–1782.

Li, J., Ma, M., Wang, Z., 2008. A two-hybrid yeast assay to quantify the effects of xenobiotics on thyroid hormone-mediated gene expression. Environ. Toxicol. Chem. 27, 159–167.

Miller 3rd, C.A., 1998. A human aryl hydrocarbon receptor signaling pathway constructed in yeast displays additive responses to ligand mixtures. Toxicol. Appl. Pharmacol. 160, 297–303.

Moreno, M., de Lange, P., Lombardi, A., Silvestri, E., Lanni, A., Goglia, F., 2008. Metabolic effects of thyroid hormone derivatives. Thyroid 18, 239–253.

Moriyama, K., Tagami, T., Akamizu, T., Usui, T., Saijo, M., Kanamoto, N., Hataya, Y., Shimatsu, A., Kuzuya, H., Nakao, K., 2002. Thyroid hormone action is disrupted by bisphenol A as an antagonist. J. Clin. Endocrinol. Metab. 87, 5185–5190.

Samuels, H.H., Tsai, J.S., Casanova, J., Stanley, F., 1974. Thyroid hormone action: in vitro characterization of solubilized nuclear receptors from rat liver and cultured GH1 cells. J. Clin. Invest. 54, 853–865.

Sap, J., Munoz, A., Damm, K., Goldberg, Y., Ghysdael, J., Leutz, A., Beug, H., Vennstrom, B., 1986. The c-erb-A protein is a high-affinity receptor for thyroid hormone. Nature 324, 635–640.

Shiraishi, F., Okumura, T., Nomachi, M., Serizawa, S., Nishikawa, J., Edmonds, J.S., Shiraishi, H., Morita, M., 2003. Estrogenic and thyroid hormone activity of a series of hydroxy-polychlorinated biphenyls. Chemosphere 52, 33–42.

Suen, C.S., Yen, P.M., Chin, W.W., 1994. In vitro transcriptional studies of the roles of the thyroid hormone (T3) response elements and minimal promoters in T3-stimulated gene transcription. J. Biol. Chem. 269, 1314–1322.

Takeshita, A., Yen, P.M., Misiti, S., Cardona, G.R., Liu, Y., Chin, W.W., 1996. Molecular cloning and properties of a full-length putative thyroid hormone receptor coactivator. Endocrinology 137, 3594–3597.

Thompson, C.C., Weinberger, C., Lebo, R., Evans, R.M., 1987. Identification of a novel thyroid hormone receptor expressed in the mammalian central nervous system. Science 237, 1610–1614.

Togashi, M., Nguyen, P., Fletterick, R., Baxter, J.D., Webb, P., 2005. Rearrangements in thyroid hormone receptor charge clusters that stabilize bound 3,5',5-triiodo-L-thyronine and inhibit homodimer formation. J. Biol. Chem. 280, 25665–25673.

Wagner, R.L., Huber, B.R., Shiau, A.K., Kelly, A., Cunha Lima, S.T., Scanlan, T.S., Apriletti, J.W., Baxter, J.D., West, B.L., Fletteric, R.J., 2001. Hormone selectivity in thyroid hormone receptors. Mol. Endocrinol. 15, 398–410.

Walfish, P.G., Yoganathan, T., Yang, Y.F., Hong, H., Butt, T.R., Stallcup, M.R., 1997. Yeast hormone response element assays detect and characterize GRIP1 coactivator-dependent activation of transcription by thyroid and retinoid nuclear receptors. Proc. Natl. Acad. Sci. USA 94, 3697–3702.

Weinberger, C., Thompson, C.C., Ong, E.S., Lebo, R., Gruol, D.J., Evans, R.M., 1986. The c-erb-A gene encodes a thyroid hormone receptor. Nature 324, 641–646.

Wikstrom, L., Johansson, C., Salto, C., Barlow, C., Campos Barros, A., Baas, F., Forrest, D., Thoren, P., Vennström, B., 1998. Abnormal heart rate and body temperature in mice lacking thyroid hormone receptor α 1. EMBO J. 17, 455–461.

Wolf, S.S., Roder, K., Schweizer, M., 1996. Construction of a reporter plasmid that allows expression libraries to be exploited for the one-hybrid system. Biotechniques 20, 568–574.

Ye, L., Li, Y.L., Mellstrom, K., Mellin, C., Bladh, L.G., Koehler, K., Garg, N., Garcia Collazo, A.M., Litten, C., Husman, B., Persson, K., Ljunggren, J., Grover, G., Sleph, P.G., George, R., Malm, J., 2003. Thyroid receptor ligands. 1. Agonist ligands selective for the thyroid receptor beta1. J. Med. Chem. 46, 1580–1588.

Yen, P.M., 2001. Physiological and molecular basis of thyroid hormone action. Physiol. Rev. 81, 1097–1142.

Zoeller, R.T., 2005. Environmental chemicals as thyroid hormone analogues: new studies indicate that thyroid hormone receptors are targets of industrial chemicals? Mol. Cell. Endocrinol. 242, 10–15.

Bioorganic & Medicinal Chemistry Letters 20 (2010) 260–265

Contents lists available at ScienceDirect

Bioorganic & Medicinal Chemistry Letters

journal homepage: www.elsevier.com/locate/bmcl

DNA methylation by dimethyl sulfoxide and methionine sulfoxide triggered by hydroxyl radical and implications for epigenetic modifications

Kazuaki Kawai, Yun-Shan Li, Ming-Fen Song, Hiroshi Kasai *

Department of Environmental Oncology, Institute of Industrial Ecological Sciences, University of Occupational and Environmental Health, 1-1, Iseigaoka, Yahatanishi-ku, Kitakyushu 807-8555, Japan

ARTICLE INFO

Article history:
Received 26 September 2009
Revised 23 October 2009
Accepted 27 October 2009
Available online 30 October 2009

Keywords:
5-Methyldeoxycytidine
Methyl radicals
Dimethylsulfoxide
Methionine sulfoxide
Epigenetic

ABSTRACT

In this Letter, we demonstrate the formation of m^5dC from dC or in DNA by dimethylsulfoxide (DMSO) and methionine sulfoxide (MetO), under physiological conditions in the presence of the Fenton reagent in vitro. DMSO reportedly affects the cellular epigenetic profile, and enhances the metastatic potential of cultured epithelial cells. The methionine sulfoxide reductase (Msr) gene was suggested to be a metastatis suppressor gene, and the accumulation of MetO in proteins may induce metastatic cancer. Our findings are compatible with these biological data and support the hypothesis that chemical cytosine methylation via methyl radicals is one of the mechanisms of DNA hypermethylation during carcinogenesis. In addition to m^5dC, the formation of 8-methyldeoxyguanosine (m^8dG) was also detected in DNA under the same reaction conditions. The m^8dG level in human DNA may be a useful indicator of DNA methylation by radical mechanisms.

Alkyl radicals, including methyl radicals, are generated from the tumor promoters, cumene hydroperoxide and *t*-butyl hydroperoxide in mouse keratinocytes, based on ESR experiments, suggesting that carbon radicals are involved in cancer induction.[1] In addition to these chemicals, the generation of methyl radicals from various carcinogens has been observed in vitro and in vivo. The metabolism of 1,2-dimethylhydrazine[2] and procarbazine[3] produces methyl radicals. Acetaldehyde generates methyl radicals by treatments with xanthine oxidase,[4] peroxynitrite,[5] and Fe^{2+}/H_2O_2.[5] The formation of a methyl radical - deoxyguanosine adduct, 8-methyl-2′-deoxyguanosine (m^8dG), has been detected in DNA after a treatment with *t*-butyl hydroperoxide and ferrous ion in vitro,[6] and after the administration of 1,2-dimethylhydrazine to rats.[7] Methylation of RNA purine bases at the C-8 position by methyl radicals has been also observed.[8] We recently reported that cytosine C-5 methylation in the monomer dC and DNA occurred via methyl radicals generated by the tumor promoters, cumene hydroperoxide and *t*-butyl hydroperoxide, in the presence of ferrous ion.[9] This discovery suggested new mechanisms of aberrant DNA hypermethylation in the epigenetic process during chemical carcinogenesis. Enzymatic DNA methylation due to the increased expression of DNA methyltransferases (DNMTs) is a widely accepted mechanism of DNA hypermethylation.[10,11] However, controversial data showing no clear association between gene hypermethylation in cancer

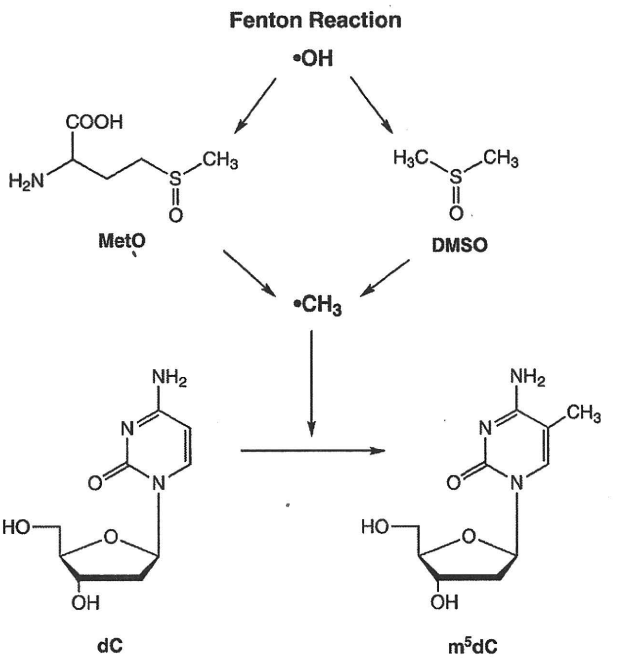

Scheme 1. Formation of m^5dC via methyl radicals by DMSO and MetO, triggered by Fenton reaction.

* Corresponding author. Tel.: +81 93 691 7469; fax: +81 93 601 2199.
E-mail address: h-kasai@med.uoeh-u.ac.jp (H. Kasai).

0960-894X/$ - see front matter © 2009 Elsevier Ltd. All rights reserved.
doi:10.1016/j.bmcl.2009.10.124

and high DNMT expression were also reported.[12,13] Therefore, it would be interesting to examine whether cytosine C-5 methylation via methyl radicals occurs by other biological/chemical systems.

Methyl radicals are reportedly generated by the reaction of OH radicals with dimethylsulfoxide (DMSO),[14] from the amino acid methionine (Met) upon gamma irradiation,[15] and by the treatment of methionine sulfoxide (MetO) with peroxynitrite.[16] Particularly, endogenous MetO formation in proteins is implicated as a pathological biomarker in relation to aging, inflammation and smoking.[17–20] It is worth mentioning that DNA hypermethylation during carcinogenesis is correlated to aging, inflammation and smoking.[21–23] DMSO also reportedly has an effect on the cellular epigenetic profile, by inducing DNA hypermethylation.[24] In this study, we examined the biological relevance of m^5dC formation in dC and DNA by methyl radicals produced from DMSO and MetO treated with a Fenton system (Scheme 1).

When dC was reacted with DMSO in the presence of Fenton reagent[8] at pH 7.3, the formation of m^5dC was clearly identified by HPLC equipped with a photodiode array UV detector (Fig. 1). The retention time and the UV spectrum of the reaction product were the same as those of the authentic m^5dC. Its formation was dependent on the concentration of DMSO (Fig. 2), and the reaction was rather rapid, due to its radical character. The reaction was approx-

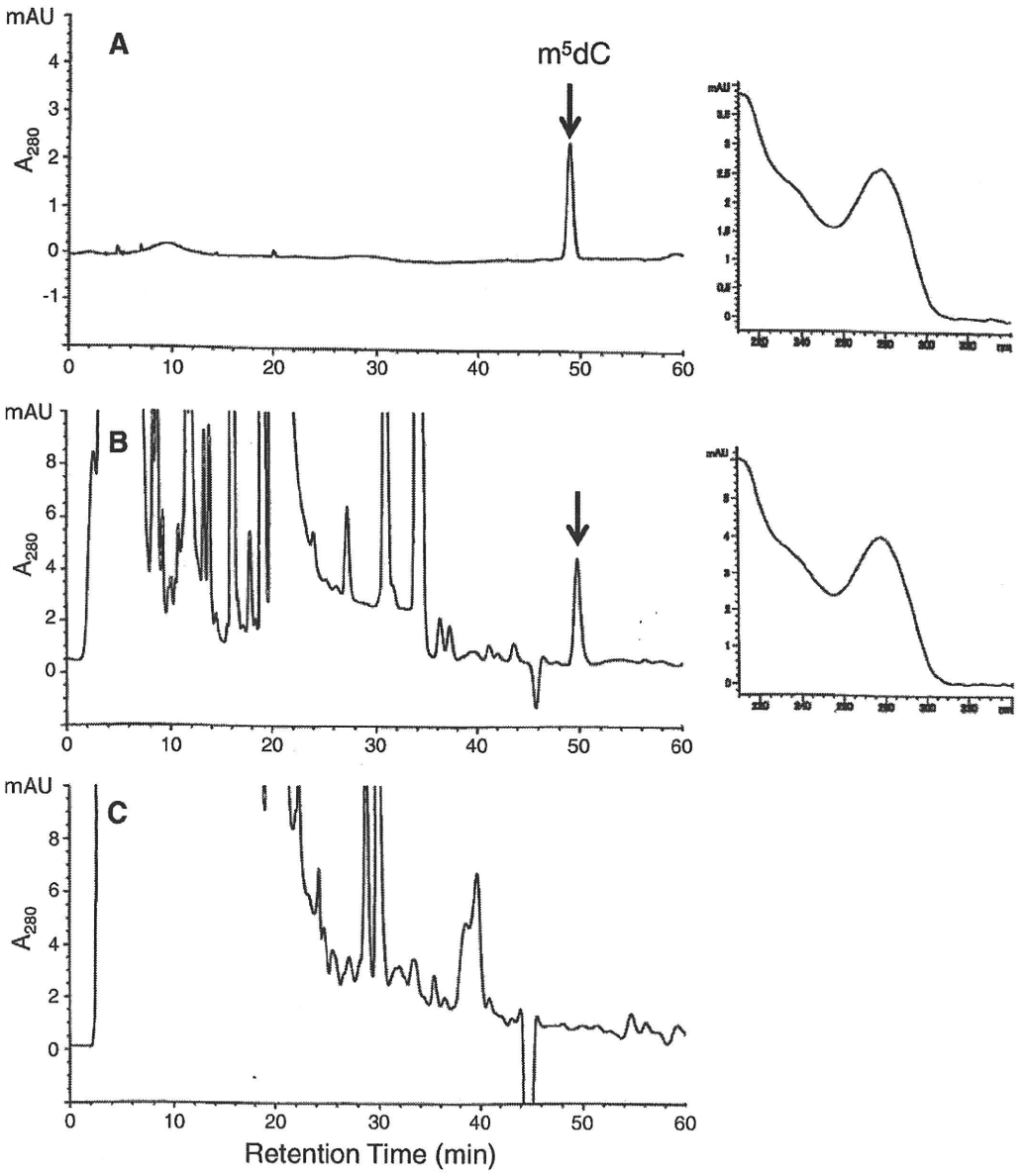

Figure 1. Detection of m^5dC in the reaction mixture of dC, DMSO and Fenton reagent by HPLC. The reaction mixture[8] (mixed under N_2 atmosphere, final volume, 0.225 ml), containing dC (final concentration, 5.46 mM), DMSO (100 mM), L-ascorbic acid (10.7 mM), EDTA·2Na (3.1 mM), $FeSO_4$ (5.3 mM), and H_2O_2 (19.6 mM) in 110 mM phosphate buffer (pH 7.3), was reacted in a sealed plastic tube (tube volume, 2 ml) by vigorous shaking at 37 °C. After a 3 h reaction, the solution was centrifuged and an aliquot of the supernatant was injected into the HPLC apparatus. (A) Chromatogram of the m^5dC standard (left) and its UV spectrum (right); (B) chromatogram of the reaction mixture (left) and UV spectrum of the peak at 50 min (right); (C) chromatogram of the control reaction mixture without DMSO.

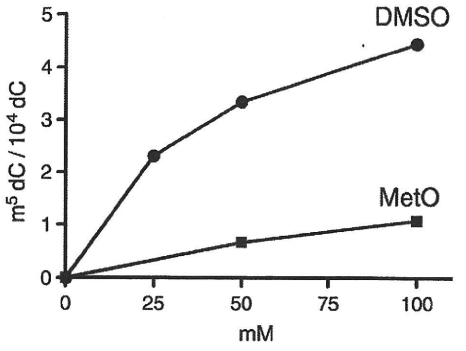

Figure 2. Dose-dependency of m^5dC formation in the dC/DMSO/Fenton reaction and the dC/MetO/Fenton reaction. The reaction conditions were the same as those in Figure 1, except that different concentrations of DMSO (25, 50 and 100 mM) and MetO (50 and 100 mM) were used. Mean values of duplicate experiments are plotted.

imately 65% complete within 5 min (data not shown). This reaction may proceed via a free radical mechanism, probably via a methyl radical. The dose-dependent formation of m^5dC from dC was also observed after a reaction with MetO plus Fenton reagent (Fig. 2).

In addition, after a double-stranded alternating copolymer, ds poly(dG-dC), was reacted with DMSO or MetO in the presence of Fenton reagent at pH 7.3, the formation of m^5dC was clearly detected in the poly(dG-dC) after the treatment, by an immuno-dot blot analysis[9,25] (Fig. 3). As a positive control, we analyzed 0.02–0.2 ng of calf thymus DNA, which contained 1.39 mol % m^5dC per P atoms. The chemiluminescence intensity increased depending upon the calf thymus DNA concentration. The control poly(dG-dC) without treatment also showed weak chemiluminescence. This means that commercial poly(dG-dC) contains a small amount of m^5dC. Since an exact quantitation was difficult with the immuno-dot blot analysis, the amount of m^5dC in the reaction mixture was further analyzed by the LC/MS/MS.

In the LC/MS analysis, the standard m^5dC exhibited an MH^+ ion at *m/z* 242, and product ion analysis from *m/z* 242 with

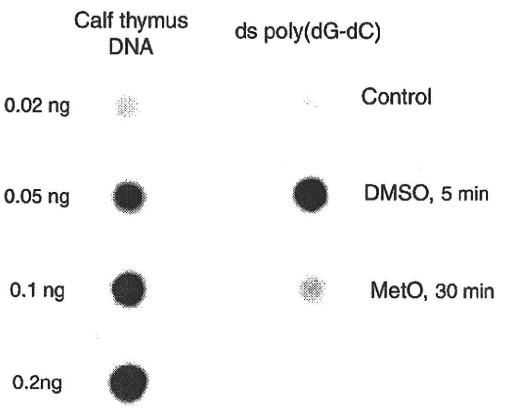

Figure 3. Detection of m^5dC in ds poly(dG-dC) by an immuno-dot blot analysis.[9,25] The reaction mixture (mixed under N_2 atmosphere, final volume, 0.45 ml) contained ds poly(dG-dC) (final concentration, 8.9 A_{260} OD units/ml), DMSO or MetO (100 mM), L-ascorbic acid (10.7 mM), EDTA·2Na (3.1 mM), $FeSO_4$ (5.3 mM), and H_2O_2 (19.6 mM), in 110 mM phosphate buffer (pH 7.3), and was reacted in a sealed plastic tube (tube volume, 2 mL) by vigorous shaking at 37 °C. After 5 min or 30 min, the ds poly(dG-dC) was recovered from the reaction mixture and was used for the analysis. As positive controls, m^5dC in various amounts of calf thymus DNA was visualized. As negative controls, untreated ds poly(dG-dC) was analyzed.

11 eV revealed a fragment BH_2^+ ion at *m/z* 126, formed by the loss of 2′-deoxyribose.[9] Therefore, the m^5dC in the reaction mixture was analyzed by LC/MS/MS, by monitoring the *m/z* 242→126 transition. In Figure 4, chromatograms of the LC/MS/MS analysis of standard m^5dC (A), poly(dG-dC)–DMSO–Fenton reagent (B), poly(dG-dC)–MetO–Fenton reagent (C), and control poly(dG-dC) without treatment (D) are shown. In both of the poly(dG-dC) samples treated with DMSO and MetO in the presence of Fenton reagent, a 242→126 transition peak appeared at 7.64 min, which is the same retention time as that of authentic m^5dC. The control poly(dG-dC) without treatment also showed a small peak (Fig. 4D). This means that the commercial poly(dG-dC) contains a small amount of m^5dC.

Based on the LC/MS/MS analysis, the yields of m^5dC in the DNA–DMSO–Fenton and DNA–MetO–Fenton reactions were calculated to be $5.00/10^4$ dC and $1.64/10^4$ dC, respectively, which are in the same range ($2–4/10^4$ dC) as the yield produced by the monomer reactions for 30 min with the DMSO- and MetO–Fenton reagents (data not shown). The high yield in DNA is unexpected, as compared to the previous result that showing the yield of m^5dC formation by a cumene hydroperoxide/Fe^{2+} system is 10-fold lower in DNA than in the dC monomer.[9] The following reasons are possible. (i) The Fenton system used in this study has higher affinity to DNA than to the monomer dC, thus generating higher levels of ·OH radicals in DNA;[26] (ii) long-range electron transfer along the DNA chain from the metal binding sites to the dC residues enhanced the yield of m^5dC in DNA.[27] Further studies with precise measurements of m^5dC using a stable isotope internal standard are required for the final conclusion.

We also analyzed the m^8dG in these reaction products by LC/MS/MS. The standard m^8dG[28] exhibited an MH^+ ion at *m/z* 282, and product ion analysis from *m/z* 282 revealed a fragment BH_2^+ ion at *m/z* 166, formed by the loss of 2′-deoxyribose. Therefore, the m^8dG was analyzed by monitoring the *m/z* 282→166 transition. In Figure 5, chromatograms of the LC/MS/MS analysis of standard m^8dG (A), poly(dG-dC)–DMSO–Fenton reagent (B), poly(dG-dC)–MetO–Fenton reagent (C), and control poly(dG-dC) without treatment (D) are shown. In the poly(dG-dC) treated with DMSO and MetO in the presence of Fenton reagent, a 282→166 transition peak appeared at 18.6 min (Fig. 5B and C), which is the same retention time as that of authentic m^8dG (Fig. 5A). The control poly(dG-dC) without treatment also displayed a small peak of m^8dG (Fig. 5D), which shows that the commercial poly(dG-dC) contains a small amount of m^8dG in addition to m^5dC. The formation of m^5dC and m^8dG in DNA polymers is summarized in Table 1. The yield of m^5dC formation in DNA was found to be 15–30-fold higher than that of m^8dG by the reaction with DMSO and MetO in the presence of Fenton reagent.

DMSO is known to induce hypermethylation of various genetic loci and affects the epigenetic profile in mouse embryoid bodies. Although those authors ascribed DNA methylation to the increase of DNMT3a activity,[24] other mechanisms of DNA methylation cannot be ruled out. DMSO also enhanced the invasiveness and metastatic potential of cultured epithelial cells, with an epigenetic effect.[29]

DNA hypermethylation is increased with age, inflammation and smoking.[21–23] The MetO/Met ratio in proteins also reportedly increased with age, inflammation and smoking.[17–20] MetO in proteins is repaired by methionine sulfoxide reductase (Msr). Three reports have suggested that the Msr gene is a tumor suppressor.[30–32]

The chemical methylation of cytosine C-5 may occur in vivo. A Met residue in a chromatin protein reportedly interacts with DNA by the intercalation of the Met side chain into a GC pair, based on NMR studies.[33] If the Met residue is oxidized to MetO, then the cytosine residues in the vicinity could undergo C-5 methylation

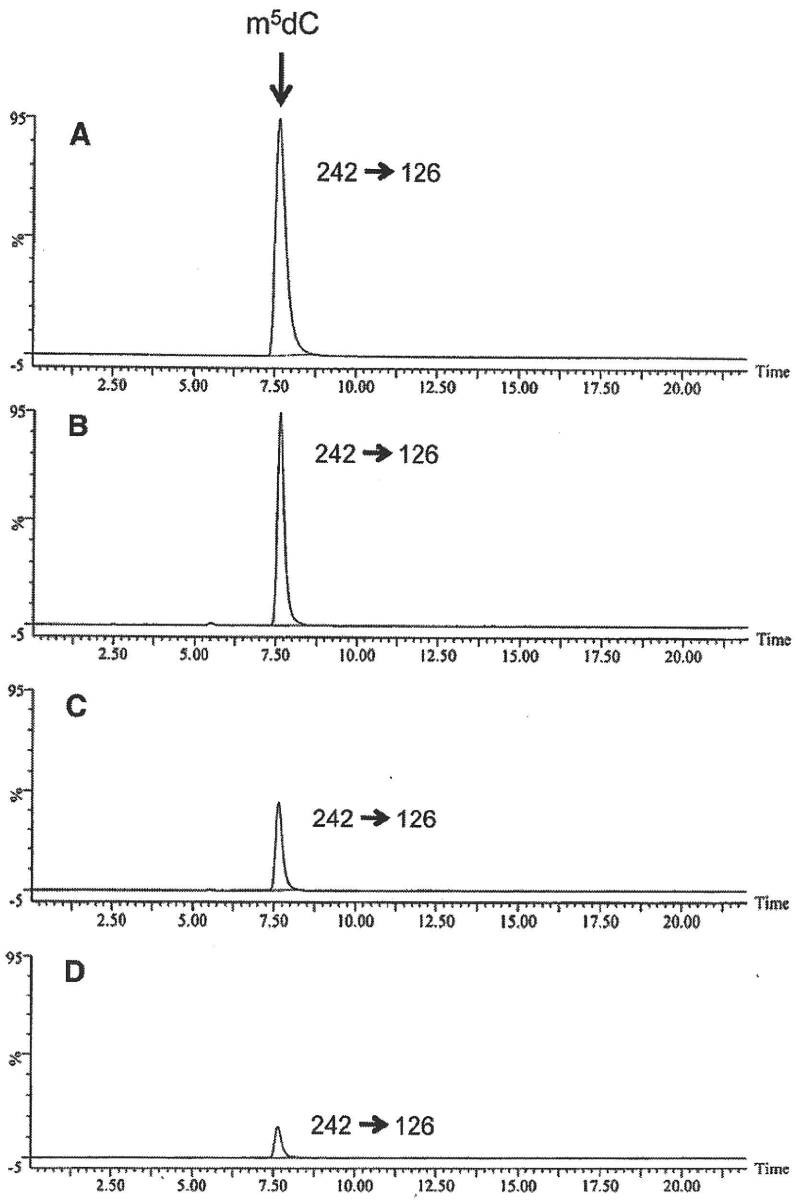

Figure 4. LC/MS/MS analysis of m^5dC in the reaction products. (A) Standard m^5dC (1.78 mg/mL); (B) hydrolysate of poly(dG-dC)/DMSO/Fenton reaction product (reaction conditions were the same as those in Figure 3, with 30 min reaction time); (C) hydrolysate of poly(dG-dC)/MetO/Fenton reaction product (reaction conditions were the same as those in Figure 3, with 30 min reaction time); and (D) control ds poly(dG-dC) without treatment. A four mL portion of each sample was injected. The transition *m/z* 242→126 was monitored. Chromatograms B, C and D are shown on the same scale.

when triggered by ·OH radicals. Various oxidized proteins and their degradation products may accumulate in the cytosol during aging and inflammation and may react with dCTP to form m^5dCTP, which could become incorporated into DNA and induce gene silencing.[34]

In the present study, in addition to m^5dC, the formation of a small amount of m^8dG was detected in the poly(dG-dC) after the treatment. The higher level of m^5dC formation than that of m^8dG may be due to a steric effect. Namely, the cytosine C-5 position may be present in a more open structure in the DNA, while the guanine C-8 is sterically hindered by the phosphate backbone.

If chemical methylation via methyl radicals is one of the mechanisms of epigenetic change during carcinogenesis, and m^8dG is formed in a specific ratio to m^5dC, then m^8dG formation analyzed by LC/MS/MS would be a good marker of chemical DNA methylation, because the background level of m^8dG would be very low, as compared to that of m^5dC, in mammalian cell DNA. Therefore, epi-mutagens inducing DNA hypermethylation can be assayed by in vitro experiments using cultured cells. The analysis of the accumulation status of m^8dG in human DNA may also be a good indicator of the increase of m^5dC in DNA by radical mechanisms, and would be useful for human cancer risk assessment.

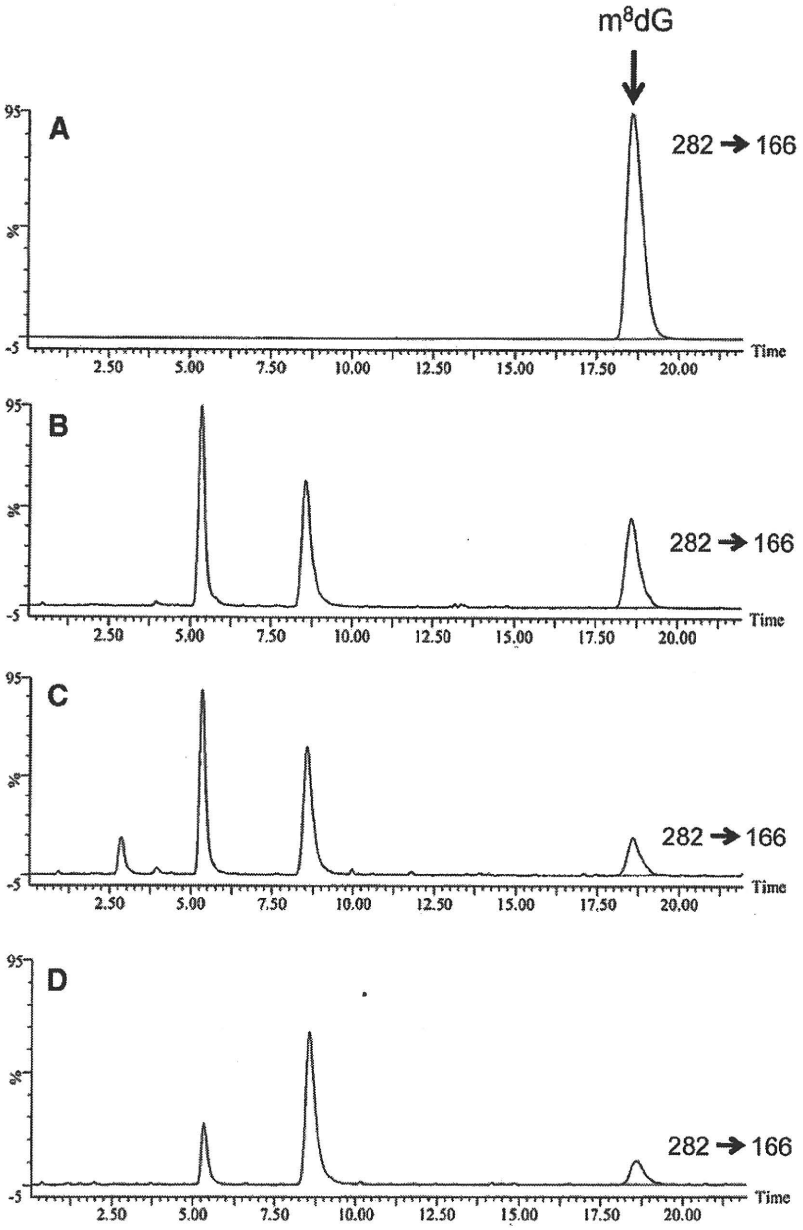

Figure 5. LC/MS/MS analysis of m^8dG in the reaction products. (A) Standard m^8dG[28] (2.08 μg/mL); (B, C, D) the same samples as B, C, D in Figure 4.

Table 1
Formation of m^5dC and m^8dG in ds poly(dG-dC) by DMSO and MetO in the presence of Fenton reagent

Reaction	$m^5dC/10^4$ dC	$m^8dG/10^4$ dG
DMSO + Fenton reagent	5.00	0.27
MetO + Fenton reagent	1.64	0.06

Acknowledgments

This work was supported by grants from the Ministry of Health, Labor and Welfare of Japan, and a grant from Asia International Educational Program for Graduate Students in the Field of Occupational Health.

References and notes

1. Taffe, B. G.; Takahashi, N.; Kensler, T. W.; Mason, R. P. *J. Biol. Chem.* **1987**, *262*, 12143.
2. Augusto, O.; Du Plessis, L. R.; Weingrill, C. L. *Biochem. Biophys. Res. Commun.* **1985**, *126*, 853.
3. Goria-Gatti, L.; Iannone, A.; Tomasi, A.; Poli, G.; Albano, E. *Carcinogenesis* **1992**, *13*, 799.
4. Nakao, L. S.; Kadiiska, M. B.; Mason, R. P.; Grijalba, M. T.; Augusto, O. *Free Radical Biol. Med.* **2000**, *29*, 721.
5. Nakao, L. S.; Ouchi, D.; Augusto, O. *Chem. Res. Toxicol.* **1999**, *12*, 1010.
6. Hix, S.; Morais Mda, S.; Augusto, O. *Free Radical Biol. Med.* **1995**, *19*, 293.
7. Netto, L. E.; RamaKrishna, N. V.; Kolar, C.; Cavalieri, E. L.; Rogan, E. G.; Lawson, T. A.; Augusto, O. *J. Biol. Chem.* **1992**, *267*, 21524.
8. Kang, J. O.; Gallagher, K. S.; Cohen, G. *Arch Biochem. Biophys.* **1993**, *306*, 178.
9. Kasai, H.; Kawai, K. *Chem. Res. Toxicol.* **2009**, *22*, 984.
10. Benbrahim-Tallaa, L.; Waterland, R. A.; Dill, A. L.; Webber, M. M.; Waalkes, M. P. *Environ. Health Perspect.* **2007**, *115*, 1454.

11. Robertson, K. D.; Uzvolgyi, E.; Liang, G.; Talmadge, C.; Sumegi, J.; Gonzales, F. A.; Jones, P. A. *Nucleic Acids Res.* **1999**, *27*, 2291.
12. Eads, C. A.; Danenberg, K. D.; Kawakami, K.; Saltz, L. B.; Danenberg, P. V.; Laird, P. W. *Cancer Res.* **1999**, *59*, 2302.
13. Ehrlich, M.; Woods, C. B.; Yu, M. C.; Dubeau, L.; Yang, F.; Campan, M.; Weisenberger, D. J.; Long, T.; Youn, B.; Fiala, E. S.; Laird, P. W. *Oncogene* **2006**, *25*, 2636.
14. Eberhardt, M. K.; Colina, R. *J. Org. Chem.* **1988**, *53*, 1071.
15. Makino, K. *J. Phys. Chem.* **1979**, *83*, 2520.
16. Nakao, L. S.; Iwai, L. K.; Kalil, J.; Augusto, O. *FEBS Lett.* **2003**, *547*, 87.
17. Wells-Knecht, M. C.; Lyons, T. J.; McCance, D. R.; Thorpe, S. R.; Baynes, J. W. *J. Clin. Invest.* **1997**, *100*, 839.
18. Onorato, J. M.; Thorpe, S. R.; Baynes, J. W. *Ann. N.Y. Acad. Sci.* **1998**, *854*, 277.
19. Hosako, M.; Ogino, T.; Omori, M.; Okada, S. *Free Radical Biol. Med.* **2004**, *36*, 112.
20. Carp, H.; Miller, F.; Hoidal, J. R.; Janoff, A. *Proc. Natl. Acad. Sci. U.S.A.* **1982**, *79*, 2041.
21. Kim, S. K.; Jang, H. R.; Kim, J. H.; Kim, M.; Noh, S. M.; Song, K. S.; Kang, G. H.; Kim, H. J.; Kim, S. Y.; Yoo, H. S.; Kim, Y. S. *Carcinogenesis* **2008**, *29*, 1623.
22. Suzuki, H.; Toyota, M.; Kondo, Y.; Shinomura, Y. *Methods Mol. Biol.* **2009**, *512*, 55.
23. Kim, J. S.; Kim, H.; Shim, Y. M.; Han, J.; Park, J.; Kim, D. H. *Carcinogenesis* **2004**, *25*, 2165.
24. Iwatani, M.; Ikegami, K.; Kremenska, Y.; Hattori, N.; Tanaka, S.; Yagi, S.; Shiota, K. *Stem Cells* **2006**, *24*, 2549.
25. Leuratti, C.; Singh, R.; Lagneau, C.; Farmer, P. B.; Plastaras, J. P.; Marnett, L. J.; Shuker, D. E. *Carcinogenesis* **1998**, *19*, 1919.
26. Floyd, R. A. *Biochem. Biophys. Res. Commun.* **1981**, *99*, 1209.
27. Arkin, M. R.; Stemp, E. D.; Pulver, S. C.; Barton, J. K. *Chem. Biol.* **1997**, *4*, 389.
28. Maeda, M.; Nushi, K.; Kawazoe, Y. *Tetrahedron* **1974**, *30*, 2677.
29. Bentel, J. M.; Rhodes, G. C.; Markus, I.; Smith, G. J. *Int. J. Cancer* **1990**, *46*, 251.
30. Bilsborough, J.; Van Pel, A.; Uyttenhove, C.; Boon, T.; Van den Eynde, B. J. *J. Immunol.* **1999**, *162*, 3534.
31. Lei, K. F.; Wang, Y. F.; Zhu, X. Q.; Lu, P. C.; Sun, B. S.; Jia, H. L.; Ren, N.; Ye, Q. H.; Sun, H. C.; Wang, L.; Tang, Z. Y.; Qin, L. X. *BMC Cancer* **2007**, *7*, 172.
32. De Luca, A.; Sacchetta, P.; Nieddu, M.; Di Ilio, C.; Favaloro, B. *BMC Mol. Biol.* **2007**, *8*, 39.
33. Allain, F. H.; Yen, Y. M.; Masse, J. E.; Schultze, P.; Dieckmann, T.; Johnson, R. C.; Feigon, J. *EMBO J.* **1999**, *18*, 2563.
34. Holliday, R.; Ho, T. *Somat. Cell Mol. Genet.* **1991**, *17*, 537.

DNA Modifications by the ω-3 Lipid Peroxidation-Derived Mutagen 4-Oxo-2-hexenal in Vitro and Their Analysis in Mouse and Human DNA

Kazuaki Kawai,[†] Pei-Hsin Chou,[‡] Tomonari Matsuda,[‡] Masaaki Inoue,[§] Kaisa Aaltonen,[∥] Kirsti Savela,[∥] Yoshikazu Takahashi,[⊥] Hikaru Nakamura,[⊥] Tomoyuki Kimura,[⊥] Takumi Watanabe,[⊥] Ryuichi Sawa,[⊥] Kazuyuki Dobashi,[#] Yun-Shan Li,[†] and Hiroshi Kasai*[,†]

Department of Environmental Oncology, Institute of Industrial Ecological Sciences, University of Occupational and Environmental Health, 1-1, Iseigaoka, Yahatanishi-ku, Kitakyushu, 807-8555, Japan, Research Center for Environmental Quality Management, Kyoto University, 1-2 Yumihama, Otsu, Shiga, 520-0811, Japan, Department of Chest Surgery, Niigata Rosai Hospital, 1-7-12 Touncho, Joetsu, Niigata, 942-8502, Japan, Risk Assessment Unit, Finnish Food Safety Authority Evira, Mustialankatu 3, FI-00790 Helsinki, Finland, Microbial Chemistry Research Center, 3-14-23, Kamiosaki, Shinagawa-ku, Tokyo, 141-0021, Japan, and Japan Bioindustry Association, Grande Building 8F, 2-26-9 Hatchobori, Chuo-ku, Tokyo 104-0032, Japan

Received October 16, 2009

4-Oxo-2-hexenal (4-OHE), which forms a 2′-deoxyguanosine (dG) adduct in a model lipid peroxidation system, is mutagenic in the Ames test. It is generated by the oxidation of ω-3 fatty acids and is commonly found in dietary fats, such as fish oil, perilla oil, rapeseed oil, and soybean oil. 4-OHE also forms adducts with 2′-deoxyadenosine (dA), 2′-deoxycytidine (dC), and 5-methyl-2′-deoxycytidine (5-Me-dC) in DNA. In this study, we characterized the structures of these adducts in detail. We measured the amounts of 4-OHE−DNA adducts in mouse organs by LC/MS/MS, after 4-OHE was orally administered to mice. The 4-OHE−dA, 4-OHE−dC, 4-OHE−dG, and 4-OHE−5-Me-dC adducts were detected in stomach and intestinal DNA in the range of 0.25−43.71/10^8 bases. After the 4-OHE administration, the amounts of these DNA adducts decreased gradually over 7 days. We also detected 4-OHE−dC in human lung DNA, in the range of 2.6−5.9/10^9 bases. No difference in the 4-OHE adduct levels was detected between smokers and nonsmokers. Our results suggest that 4-OHE−DNA adducts are formed by endogenous as well as environmental lipid peroxides.

Introduction

The oxidation of unsaturated fatty acids generates toxic reactive aldehydes, such as 4-hydroxy-2-nonenal, malondialdehyde, acrolein, and crotonaldehyde (*1*−*3*). These aldehydes directly react with DNA and are considered to contribute to mutagenesis and carcinogenesis (*4*−*6*). Unsaturated aldehydes are generated not only as pollutants by heat decomposition of fat (*7*), cigarette smoking (*8*), and other environmental factors but also as oxidation products of membrane lipids in vivo (*9*). Although the exact mechanism is not clear, these environmental and endogenous aldehydes may play a role in tissue toxicity and carcinogenicity. Recently, we found a novel mutagenic oxidation product, 4-oxo-2-hexenal (4-OHE),[1] in the lipid peroxidation model reaction (*10*−*13*). Namely, when dG was reacted with linolenic acid methyl ester and Fe-containing hemin, as a catalyst for lipid peroxidation, six dG adducts were detected by an HPLC analysis. One of them was the 4-OHE−dG adduct (dG*), and thus 4-OHE was considered to be a new mutagen produced by ω-3 lipid peroxidation. 4-OHE is mutagenic in the *Salmonella typhimurium* strains TA 104 and TA 100, and it covalently modifies dC, dG, and 5-Me-dC to form substituted etheno type adducts. Our new results revealed that 4-OHE could also modify dA to produce an etheno-dA derivative. These 4-OHE adducts were detected after DNA was treated with 4-OHE in vitro. These results are basically similar to those from structural studies on adduct formation by 4-oxo-2-nonenal with DNA or nucleosides in vitro (*14*−*17*).

Because the diet plays a pivotal role in the development of human cancer (*18*), it is important to identify whether this novel mutagen, 4-OHE, exists in foods. Actually, 4-OHE was present in commercial perilla oil, the edible part of broiled fish, and various fried foods in the range of 1−70 μg/g (*12*). Furthermore, 4-OHE was detected by a GC/MS analysis of the ethyl acetate trap of the smoke released during the broiling of fish. Some epidemiological and experimental studies have demonstrated that cooking oil vapors may be related to cancer risk (*19*, *20*). In general, these types of DNA adducts are considered as promutagenic lesions and can lead to the initiation of carcinogenesis. The detection and quantitation of these adducts as markers for the initiation of cancer may be useful for cancer risk assessment. The in vivo formation of the DNA adducts of 4-OHE has not

* To whom correspondence should be addressed. Tel: +81-93-691-7469. Fax: +81-93-601-2199. E-mail: h-kasai@med.uoeh-u.ac.jp.
[†] University of Occupational and Environmental Health.
[‡] Kyoto University.
[§] Niigata Rosai Hospital.
[∥] Finnish Food Safety Authority Evira.
[⊥] Microbial Chemistry Research Center.
[#] Japan Bioindustry Association.

[1] Abbreviations: 4-OHE, 4-oxo-2-hexenal; HRESI-MS, high-resolution electrospray ionization mass spectrometry; ESI-MS, electrospray ionization mass spectrometry; FAB-MS, fast atom bombardment mass spectrometry; ORTEP, Oak Ridge Thermal Ellipsoid Program; COSY, correlation spectroscopy; HMQC, heteronuclear multiple quantum correlation; HMBC, heteronuclear multiple bond correlation; NOESY, nuclear Overhauser effect spectroscopy.

10.1021/tx9003819
Published on Web 01/07/2010

previously been demonstrated, except in our previous brief report (*10*). In the present study, we report the detailed structural characterization of the 4-OHE−dA, 4-OHE−dC, and 4-OHE−5-Me-dC adducts and the detection of 4-OHE adducts in the organ DNA from 4-OHE-exposed mice and in human lung DNA by an LC/MS/MS method.

Materials and Methods

Materials. Deoxycytidine hydrochloride and deoxyadenosine were obtained from Yoshitomi Pharmaceutical Co., which is presently Yoshitomiyakuhin Co. (Osaka, Japan). 5-Methyl-2′-deoxycytidine and 2′-deoxycytidine 3′-monophosphate sodium salt were purchased from Sigma Chemical Co. (St. Louis, MO). Stable isotope-labeled compounds, 2′-deoxyadenosine (U-$^{15}N_5$, 98%) and 2′-deoxycytidine (U-$^{15}N_3$, 96−98%), were obtained from Cambridge Isotope Laboratories, Inc. (MA). 4-OHE was synthesized according to a previously described method (*11*).

Spectra Measurements. The mass spectra of the adducts were recorded with JEOL JMS-DX-303 (fast atom bombardment mass spectrometry, FAB-MS), JEOL JMS-T100LC (electrospray ionization mass spectrometry, ESI-MS), and Thermo Fisher Scientific LTQ Orbitrap (ESI-MS/MS) mass spectrometers. ^1H and ^{13}C NMR spectra were measured with a JEOL JNM-ECA600 spectrometer, using tetramethylsilane (TMS) as an internal reference.

X-ray Crystallography of 4-OHE-dC (dC*). A colorless prismatic crystal of dC*, with approximate dimensions of 0.40 mm × 0.10 mm × 0.05 mm, was chosen for X-ray crystallography. The crystal data are as follows: empirical formula, $C_{15}H_{19}N_3O_5$; FW, 321.33; crystal system, orthorhombic; lattice parameters: a = 8.4034 (13) Å, b = 34.9581 (18) Å, c = 5.1410 (17) Å, and V = 1510.3 (6) Å^3; space group, $P2_12_12_1$; Z value, 4; D_{calcd}, 1.413 g/cm^3; and μ(Cu Kα), 9.027 cm^{-1}. X-ray crystallographic measurements were performed on a Rigaku AFC7R diffractometer, with graphite monochromated Cu Kα radiation and a rotating anode generator. Data processing was performed using CrystalStructure 3.8.2 (Rigaku).

Preparation of 8-(2-Oxobutyl)-3,*N*4-etheno-dC (dC*). Deoxycytidine hydrochloride (52.8 mg, 0.200 mmol) and 4-OHE (67.2 mg, 0.599 mmol) were dissolved in 24 mL of 50 mM sodium phosphate buffer (pH 7.4) containing 10% ethanol and incubated for 5 days at room temperature. The product (retention time, 42.5−43.6 min) was separated by repeated rounds of HPLC [column: CAPCELL PAK C18, 5 μm, 10 mm × 250 mm, Shiseido Fine Chemicals, Japan; elution: 0−40 min, linear gradient of methanol (15−30%); 40−60 min, 30% methanol; flow rate, 3 mL/min]. The yield was 20.5 mg (32.0%).

Preparation of 8-(2-Oxobutyl)-3,*N*4-etheno-5-methyl-dC (5-Me-dC*). 5-Methyl-2′deoxycytidine (50.3 mg, 0.209 mmol) and 4-OHE (25.8 mg, 0.230 mmol) were dissolved in 25 mL of 50 mM sodium acetate (pH 5.0) containing 10% ethanol and incubated for 5 days at room temperature. The product (retention time, 52.4−54.2 min) was separated by repeated rounds of HPLC (the same conditions as above). The yield was 28.8 mg (41.0%).

Preparation of 11-(2-Oxobutyl)-1,*N*6-etheno-dA (dA*). Deoxyadenosine (100 mg, 0.398 mmol) and 4-OHE (126 mg, 1.124 mmol) were dissolved in 100 mL of 5% aqueous ethanol and incubated for 15 h at 50 °C. The product (retention time, 33.7−35.5 min) was separated by repeated rounds of HPLC (column: CAPCELL PAK C18, 5 μm, 10 mm × 250 mm; elution: 12% aqueous acetonitrile; flow rate, 3 mL/min). The yield was 20.0 mg (14.5%).

Preparation of Isotope-Labeled dC* and dA*. Stable isotope-labeled dC* and dA* were prepared from 2′-deoxyadenosine (U-$^{15}N_5$, 98%) and 2′-deoxycytidine (U-$^{15}N_3$, 96−98%) by a similar procedure as described above. Briefly, ^{15}N-deoxycytidine (5 mg) and 4-OHE (8 mg) were dissolved in 1 mL of 50 mM sodium phosphate buffer (pH 7.4) containing 10% ethanol and incubated for 3 days at room temperature. The product ^{15}N-dC* (retention time, 27.2 min) was separated by repeated rounds of HPLC [column: CAPCELL PAK C18, 5 μm, 4.6 mm × 250 mm; elution: 0−30 min, linear gradient of methanol (15−30%); flow rate, 1 mL/min]. For the preparation of ^{15}N-dA*, ^{15}N-deoxyadenosine (5.8 mg) and 4-OHE (10 mg) were dissolved in 1 mL of 10% aqueous ethanol and incubated for 10 h at 50 °C. The product (retention time, 20.6 min) was separated by repeated rounds of HPLC (column: CAPCELL PAK C18, 5 μm, 4.6 mm × 250 mm; elution: 12% aqueous acetonitrile; flow rate, 1 mL/min).

Reaction of 4-OHE with Calf Thymus DNA in Vitro. 4-OHE (5 μL) was added to calf thymus DNA (1 mg, heat denatured in boiling water for 10 min) in 1 mL of phosphate buffer (50 mM, pH 7.0) containing 17% ethanol. The reaction mixture was incubated at 37 °C for 16 h. The DNA was precipitated by adding 2.4 mL of cold ethanol and 20 mL of cold 2 M sodium acetate. After the solution was centrifuged, the supernatant was removed, and the DNA pellet was washed with 1 mL of cold 70% ethanol. The DNA pellet was dried under reduced pressure.

Hydrolysis of 4-OHE-Modified Calf Thymus DNA. The modified DNA was dissolved in 0.3 mL of water. A 100 μL aliquot of 0.5 M Tris-HCl (pH 8.0) and 5 mM $MgCl_2$, 3 μL of snake venom phosphodiesterase I (100 units/mL, Funakoshi Co., Ltd., Tokyo, Japan), and 4 mL of alkaline phosphatase (1 u/μL, Roche Diagnostics Gmbh, Mannheim, Germany) were added to the DNA solution. The DNA was hydrolyzed at 37 °C overnight and filtered through a 0.45 μm filter before analysis by HPLC.

Treatment of Animals. Five week old female ICR mice were obtained from SLC Japan Inc. (Shizuoka, Japan). Animals were maintained in a temperature- and photoperiod (12 h/day)-controlled room. The animals were fed with the standard diet CE-2 from CLEA Japan Inc. (Tokyo). Oral doses of 3 mg 4-OHE/mouse dissolved in corn oil were administered i.g. to 6 week old female ICR mice. Control animals were treated with corn oil only. The mice were sacrificed under deep ether anesthesia at different times, ranging from 24 h to 7 days. Harvested were the following organs: esophagus, stomach, liver, kidney, small intestine, and large intestine. The digestive tract organs were washed with 70% ethanol and a sodium chloride solution. The organs were stored at −80 °C. All of the animal experimental procedures were performed in accordance with the guidelines for the care and use of laboratory animals at our university.

Preparation of Human Lung Tissues. Lung samples were obtained during surgery for 10 lung cancer patients at the Niigata Rosai Hospital (Niigata, Japan). After resection, noncancerous lung tissues were removed, frozen immediately in liquid nitrogen, and stored at −80 °C.

DNA Extraction. The nuclear DNA of the mouse tissue and the human lung was isolated by the sodium iodide method, using a DNA Extraction WB Kit (Wako Pure Chemical Industries, Ltd., Osaka, Japan). To avoid oxidative DNA artifacts, 1 mM desferal (deferoxamine mesylate, Sigma Chemical Co.) was added to the lysis solution for the tissue homogenization and DNA extraction. A 50 mg portion of tissue was homogenized with a Teflon glass homogenizer, in 1 mL of ice-cold lysis solution. Subsequent DNA isolation was performed according to the manufacturer's instructions.

DNA Hydrolysis. The isolated DNA was enzymatically digested as follows: Each DNA sample (50 μg for the mouse tissues and 25 μg for the human lung samples) was mixed with 36 μL of digestion buffer (17 mM sodium succinate and 8 mM calcium chloride, pH 6.0) containing 45 units of micrococcal nuclease (Worthington, United States), 0.15 units of spleen phosphodiesterase (Worthington), and two stable isotope internal standards, [$^{15}N_3$]-dC* (20 fmol) and [$^{15}N_5$]-dA* (20 fmol). After 3 h of incubation at 37 °C, 3 units of alkaline phosphatase (Sigma, United States), 10 μL of 0.5 M Tris-HCl (pH 8.5), 5 μL of 20 mM zinc sulfate, and 49 μL of Milli-Q water were added, and the mixture was incubated for 3 h at 37 °C. After this incubation, the mixture was concentrated to 10−20 μL by a Speed-Vac concentrator, and 100 μL of methanol was added to precipitate the protein. After centrifugation, the methanol fraction (supernatant) was transferred to a new Eppendorf tube. The precipitate was extracted with 100 μL of methanol, and the methanol fractions were combined and evaporated to dryness.

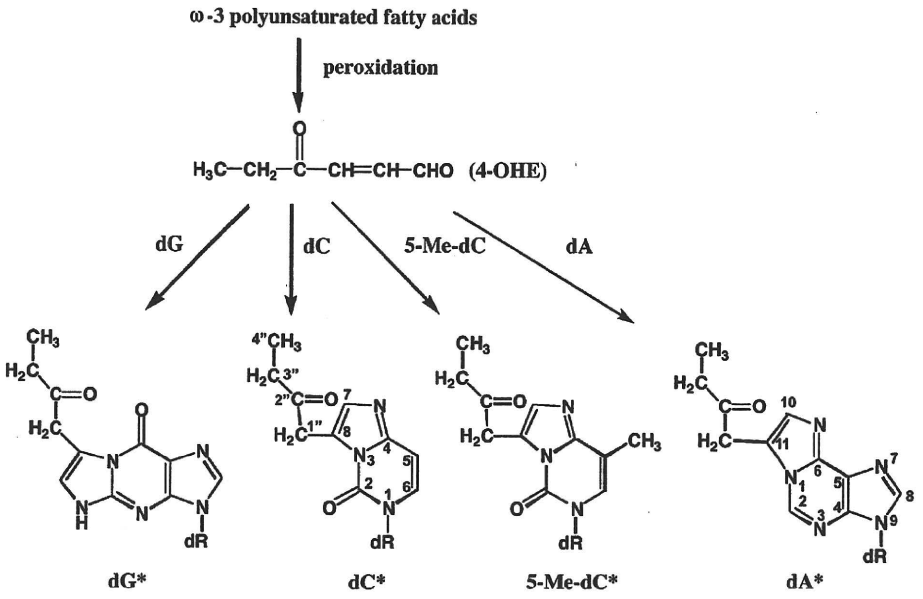

Figure 1. Structures of 4-OHE–DNA adducts.

Samples were resuspended in 50 μL of Milli-Q water before LC/ESI-MS/MS analysis.

LC/ESI-MS/MS Analyses. The LC/MS/MS analysis was performed using a Quattro Ultima Pt triple stage quadrupole mass spectrometer (Waters-Micromass, United States) equipped with a Shimadzu LC system (Shimadzu, Japan). An aliquot of each sample (40 μL) was injected and separated by a Shim-pack XR-ODS column (3.0 mm × 75 mm, Shimadzu, Japan). The column was eluted with a linear gradient of 15–80% methanol in water from 0 to 15 min at a flow rate of 0.2 mL/min and then was switched back to the initial condition of 15% methanol in water from 15 to 27 min. Mass spectral analysis was performed in the positive ion mode, using nitrogen as the nebulizing gas. Experimental conditions were set as follows: ion source temperature, 130 °C; desolvation temperature, 380 °C; cone voltage, 35 V; desolvation gas flow rate, 700 L/h; and cone gas flow rate, 35 L/h. Argon was used as the collision gas. The collision energy and characteristic reactions (base ion→product ion) monitored for the different DNA adducts are as follows: dC* (10 eV, 321.8→205.8), [$^{15}N_3$]-dC* (10 eV, 324.8→208.6), 5-Me-dC* (20 eV, 335.9→220.0), dA* (10 eV, 345.8→229.8), [$^{15}N_5$]-dA* (10 eV, 351.0→234.8), and dG* (20 eV, 362.0→245.9).

The amount of each DNA adduct was quantified by calculating the peak area ratio of the target DNA adduct and its specific internal standard ([$^{15}N_3$]-dC* was used for dC* and 5-Me-dC*, and [$^{15}N_5$]-dA* was used for dA* and dG*). Calibration curves were obtained using authentic standards spiked with isotopically labeled internal standards. The concentration of 2′-deoxyguanosine (dG) in each DNA sample was also monitored by the SPD-10Avp UV–visible detector in the Shimadzu LC system, and the adduct levels in each sample were calculated using the amount of dG. The number of DNA adducts per 10^9 bases was calculated by the following equation: number of DNA adducts per 10^9 bases = adduct level (fmol/μmol dG) × 0.218(μmol dG/μmol dN), as described previously (*21*).

The signal-to-noise ratio (S/N: peak to peak) of the adduct peak was calculated by using the Masslynx V4.0 software. The detection limits of the adducts, for which the peaks were expected to have an S/N of 3, were 0.13 (dG*), 0.35 (dA*), 0.41 (Me-dC*), and 0.08 fmol (dC*). This sensitivity was sufficient to detect 0.5–2.7 adducts per 10^9 bases when using 50 μg of DNA. The quantification limits of the peaks that were expected to have an S/N of 10 were also estimated to be 0.26 (dG*), 0.92 (dA*), 0.87 (Me-dC*), and 0.23 fmol (dC*).

Table 1. NMR Data of dC* in DMSO-d_6[a]

position	δ_C (ppm)	δ_H (ppm)	multiplicity, *J* (Hz)
2	146.8		
4	145.1		
5	98.9	6.62	d, 8.1
6	127.8	7.61	d, 8.1
7	132.6	7.11	s
8	123.0		
1′	84.7	6.30	t, 6.8
2′	40.0	2.14	m
3′	70.4	4.26	m
3′-OH		5.26	br
4′	87.6	3.81	q, 3.7
5′	61.2	3.56	dd, 3.7, 12.2
		3.60	dd, 3.7, 12.2
5′-OH		5.13	br
1″	38.7	4.11	d, 17.7
		4.15	d, 17.7
2″	206.7		
3″	34.5	2.54	q, 7.3
4″	7.6	0.95	t, 7.3

[a] Chemical shifts in ppm from TMS as an internal standard.

Results

Structure Confirmation of 4-OHE Adducts with dC, 5-Me-dC, and dA. 4-OHE reacts not only with dG but also with dC, 5-Me-dC, and dA to yield adducts (dC*, 5-Me-dC*, and dA*). The structures of dC*, 5-Me-dC*, and dA* were determined as shown in Figure 1, mainly by the MS, NMR, and X-ray crystallography data. ^1H and ^{13}C NMR data for these synthetic compounds are provided in Tables 1–3.

The molecular formula of dC* is consistent with $C_{15}H_{19}N_3O_5$, as determined by high-resolution electrospray ionization mass spectrometry (HRESI-MS) [positive ion mode, *m/z* 344.1192 $(M + Na)^+$ 344.1222 calcd for $C_{15}H_{19}N_3O_5Na$]. The HRESI-MS/MS spectrum of *m/z* 322.1 revealed product ions at *m/z* 206.0923 (Δ −0.11 mDa as $C_{10}H_{12}N_3O_2$: base + H_2), *m/z* 150.0659 (Δ −0.31 mDa $C_7H_8N_3O$: base + H_2 − C_2H_5CO), and *m/z* 121.0631 and *m/z* 57.0332 (Δ −0.25 mDa C_3H_5O: etheno ring side chain). The UV λ_{max} in H_2O was 277 nm (ε 11460). The ^1H and ^{13}C NMR spectra showed additional characteristic signals: CH_2 (δ_H 4.11 and 4.15, δ_C 38.7), C=O (δ_C 206.7), CH_2 (δ_H 2.54, δ_C 34.5), and CH_3 (δ_H 0.95, δ_C 7.6), as compared with those of dC (Table 1). dC* generated a highly

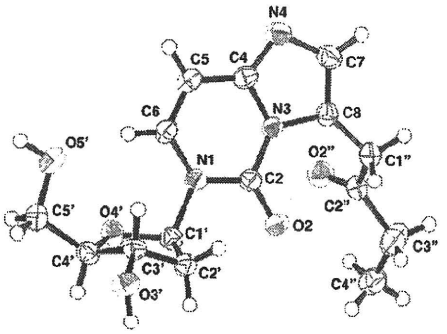

Figure 2. Crystal structure of dC*.

Table 2. NMR Data of 5-Me-dC* in DMSO-d_6[a]

position	δ_C (ppm)	δ_H (ppm)	multiplicity, J (Hz)
2	146.7		
4	146.0		
5	107.2		
5-CH_3	12.8	2.14	brd, 1.0
6	124.2	7.42	brq, 1.0
7	132.4	7.11	s
8	123.5		
1′	84.4	6.30	t, 6.8
2′	39.8	2.12	m
3′	70.4	4.26	m
3′-OH		5.26	d, 4.3
4′	87.5	3.79	dd, 3.7
5′	61.3	3.56	dt, 4.3, 12.1
		3.62	ddd, 3.7, 5.0, 12.1
5′-OH		5.06	t, 5.2
1″	38.7	4.10	d, 17.7
		4.15	d, 17.7
2″	206.7		
3″	34.5	2.53	q, 7.3
4″	7.6	0.95	t, 7.3

[a] Chemical shifts in ppm from TMS as an internal standard.

crystalline product, and thus, further structure elucidation was performed by X-ray crystallography. The compound was recrystallized by an ethanol:water (1:1) solvent system and yielded colorless prisms. An Oak Ridge Thermal Ellipsoid Program (ORTEP) drawing of dC* is shown in Figure 2. The sugar of dC* adopts the C(3′)-endo conformation, and the glycosidic torsion is in the anti form.

The molecular formula of 5-Me-dC* is consistent with $C_{16}H_{21}N_3O_5Na$, as determined by HRESI-MS [positive ion mode, m/z 358.1372, $(M + Na)^+$ 358.1379 calcd for $C_{15}H_{19}N_3O_5Na$]. The HRESI-MS/MS spectrum of m/z 336.2 revealed product ions at m/z 220.1079 (Δ −0.15 mDa as $C_{11}H_{14}N_3O_2$: base + H_2), m/z 164.0816 (Δ −0.26 mDa as $C_8H_{10}N_3O$: base + H_2 − C_2H_5CO), and m/z 135.0788, m/z 108.0679, and m/z 57.0333 (Δ −0.23 mDa as C_3H_5O: etheno ring side chain). The UV λ_{max} in H_2O was 278 nm (ε 11930). The ^1H and ^{13}C NMR spectra showed almost the same additional characteristic signals of dC*: CH_2 (δ_H 4.10 and 4.15, δ_C 38.7), C=O (δ_C 206.7), CH_2 (δ_H 2.53, δ_C 34.5), and CH_3 (δ_H 0.95, δ_C 7.6), as compared with those of 5-Me-dC (Table 2). Further structure determination was accomplished by various two-dimensional NMR techniques, such as correlation spectroscopy (COSY), heteronuclear multiple quantum correlation (HMQC), and heteronuclear multiple bond correlation (HMBC), as summarized in Figure 3. The 2-oxo-butyl side chain was attached to C-8 of the imidazole ring, as confirmed by $^1H-^{15}N$ HMBC, where cross-peaks were observed between H-1″ and N-3.

The molecular formula of dA* is consistent with $C_{16}H_{19}N_5O_4$, as determined by HRESI-MS [positive ion mode, m/z 368.1320, $(M + Na)^+$ 368.1329 calcd for $C_{16}H_{19}N_5O_4Na$]. The UV λ_{max}

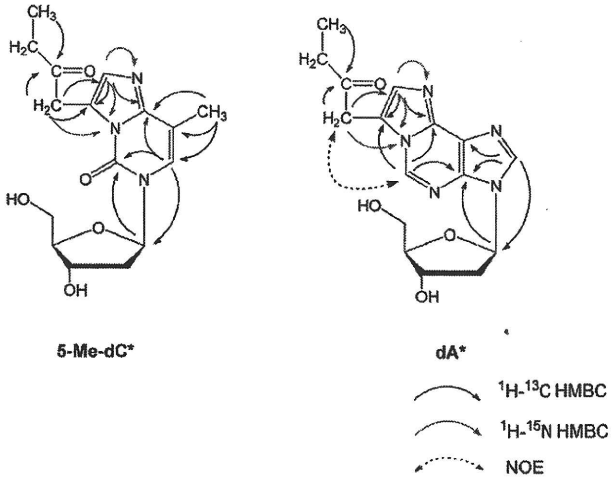

Figure 3. Selected 2D NMR results of 5-Me-dC* and dA*.

Table 3. NMR Data of dA* in DMSO-d_6[a]

position	δ_C (ppm)	δ_H (ppm)	multiplicity, J (Hz)
2	135.8	8.98	s
4	137.8		
5	123.1		
6	140.7		
8	139.8	8.51	s
10	131.8	7.34	s
11	118.5		
1′	84.0	6.47	t, 6.5
2′	39.7	2.36	ddd, 3.4, 6.5, 13.4
		2.75	dt, 6.5, 13.4
3′	70.7	4.44	m
3′-OH		5.35	d, 4.1
4′	88.0	3.89	dt, 3.1, 5.0
5′	61.7	3.54	dt, 5.0, 11.7
		3.63	dt, 5.0, 11.7
5′-OH		4.96	t, 5.0
1″	36.8	4.33	s
2″	206.7		
3″	34.5	2.65	q, 7.3
4″	7.5	0.97	t, 7.3

[a] Chemical shifts in ppm from TMS as an internal standard.

values in H_2O were 232 (ε 25800), 270 (ε 5980), and 279 nm (ε 6080). The HRESI-MS/MS spectrum of m/z 346.2 revealed product ions at m/z 230.1035 (Δ −0.18 mDa as $C_{11}H_{12}N_5O$: base + H_2) and m/z 173.0694 (Δ −0.17 mDa as $C_8H_7N_5$: base + H_2 − C_2H_5CO). The ^1H and ^{13}C NMR spectra showed additional characteristic signals: CH_2 (δ_H 4.33, δ_C 36.8), C=O (δ_C 206.7), CH_2 (δ_H 2.65, δ_C 34.5), and CH_3 (δ_H 0.97, δ_C 7.5), as compared with those of dA (Table 3). Further structure determination was accomplished by various two-dimensional NMR techniques, such as COSY, HMQC, HMBC, and nuclear Overhauser effect spectroscopy (NOESY), as summarized in Figure 3. The $^1H-^{13}C$ HMBC spectrum of dA* is shown in Figure 4. The 2-oxo-butyl side chain was attached to C-11 of the imidazole ring, as confirmed by a NOE observed between H-2 and H-1″, and the cross-peaks observed between H-1″ and N-1 by $^1H-^{15}N$ HMBC.

Reaction of 4-OHE with Calf Thymus DNA in Vitro. The 4-OHE−DNA adducts formed by the reaction of 4-OHE and calf thymus DNA in vitro were analyzed by HPLC (Figure 5). They were efficiently formed in heat-denatured calf thymus DNA (ss DNA). The yield of the 4-OHE−DNA adducts was about 50 times higher in ss DNA than in ds DNA (data not shown). At a physiological pH, the efficient formation of dC* and 5-Me-dC* was observed (Table 4). This may be due to the higher reactivity of 4-OHE with dC and 5-Me-dC than with dG and dA, rather than steric reasons.